J. Fluid Mech. (2013), *vol.* 717, *pp.* 612–642.
doi:10.1017/jfm.2012.598

Nonlinear resonant interactions of interfacial waves in horizontal stratified channel flows

Bryce K. Campbell and Yuming Liu†

Department of Mechanical Engineering, Center for Ocean Engineering, Massachusetts Institute of Technology, Cambridge, MA 02139, USA

(Received 21 November 2011; revised 19 October 2012; accepted 2 December 2012; first published online 1 February 2013)

We consider the problem of nonlinear resonant interactions of interfacial waves with the presence of a linear interfacial instability in an inviscid two-fluid stratified flow through a horizontal channel. The resonant triad consists of a (linearly) unstable wave and two stable waves, one of which has a wavelength that can be much longer than that of the unstable component. Of special interest is the development of the long wave by energy transfer from the base flow due to the coupled effect of nonlinear resonance and interfacial instability. By use of the method of multiple scales, we derive the interaction equations which govern the time evolution of the amplitudes of the interacting waves including the effect of interfacial instability. The solution of the evolution equations shows that depending on the flow conditions, the (stable) long wave can achieve a bi-exponential growth rate through the resonant interaction with the unstable wave. Moreover, the unstable wave can grow unboundedly even when the nonlinear self-interaction effect is included, as do the stable waves in the associated resonant triad. For the verification of the theoretical analysis and the practical application involving a broadbanded spectrum of waves, we develop an effective direct simulation method, based on a high-order pseudo-spectral approach, which accounts for nonlinear interactions of interfacial waves up to an arbitrary high order. The direct numerical simulations compare well with the theoretical analysis for all of the characteristic flows considered, and agree qualitatively with the experimental observation of slug development near the entrance of two-phase flow into a pipe.

Key words: geophysical and geological flows, instability, stratified flows

1. Introduction

In this work, we investigate a nonlinear mechanism for the generation and evolution of long waves on the interface in a two-layer density-stratified flow through a horizontal channel under the influence of a linear interfacial instability and nonlinear resonant wave interactions. This work is motivated by the observations of a unique class of large wave disturbances which can occur in horizontal channels and pipes. Under certain flow conditions, it is possible for short waves to form at the interface and grow into large-amplitude long waves which bridge the channel and touch the top trapping long bubbles of one fluid within the other. This phenomena, known as slug flow, has been well documented experimentally, but theoretically understanding the underlying mechanisms and properly defining the critical flow conditions for slug formation remains an active area of research.

† Email address for correspondence: yuming@mit.edu

Early theoretical work on slug prediction was based on the classical Kelvin–Helmholtz instability criteria for infinitesimal waves at the interface of a stratified flow. Experimental trials found that this criteria made poor predictions of the upper fluid velocity at which the slug transition occurs. Numerous works were dedicated to modifying that criteria by including additional physical effects such as the interfacial and wall friction (e.g. Lin & Hanratty 1986; Barnea & Taitel 1993) and normal viscous stresses at the interface (e.g. Funada & Joseph 2001). The work by Taitel & Dukler (1976) attempted to improve the predictions by examining the effects of finite-amplitude waves. However, that work simply assumed the existence of a finite-amplitude state within the channel and did not examine the mechanism(s) leading to the wave's formation. The results of these previous efforts have been a wide range of stability predictions as demonstrated in the survey by Mata *et al.* (2002).

One commonality with these methods was that the transition criteria which were developed were used to determine whether long-wavelength disturbances were unstable in the stratified flow. Experimental observation has shown that slugs form through either the evolution of short waves into large-amplitude long waves or wave coalescence. Fan, Lusseyran & Hanratty (1993) studied the formation of slugs in horizontal pipes and used power spectra from the wave heights along the pipe to demonstrate the presence of a mechanism which was creating a cascade of energy from short to long-wavelength components. Jurman, Deutsch & McCready (1992), carried out experiments for two-fluid stratified flows through a horizontal channel and used the bicoherence spectrum to examine the spectral evolution of the interface. Strong energy transfer from short to long waves was observed and in some cases there was a strong subharmonic energy transfer. These characteristic behaviours are impossible to see from linear theory because it does not permit wave interactions. This suggests that nonlinear interactions, which have been neglected from the majority of the previous studies, may play a dominant role in the interfacial evolution and must be accounted for in predicting the development of large-amplitude long interfacial waves in stratified flows.

Nayfeh & Saric (1972) used the method of multiple scales to develop a third-order amplitude equation which governed the nonlinear evolution of a finite-amplitude wave on the interface of a two-fluid density stratified flow of infinite depth. Their analysis considered a single linearly unstable mode and found that depending on the flow conditions it was possible for the nonlinear solution to grow unboundedly. Similar work was also carried out by Drazin (1970) and Maslowe & Kelly (1970). Pedlosky (1975) also studied the nonlinear evolution of an interface in the presence of a linear instability within the context of baroclinic waves. These methods provided a basis for understanding the nonlinear effects upon the growth of linearly unstable waves.

While the results of Nayfeh & Saric (1972) provided the methods necessary to examine the nonlinear evolution of linearly unstable waves, the results lacked the means to generate large-amplitude long waves from unstable short waves. The observations of energy transfer across the wave spectrum is similar to the effects observed in ocean surface wave environments. Phillips (1960) was the first to consider the effects of weak, nonlinear resonant wave–wave interactions in an ocean wave field. His work determined that these nonlinear interactions were responsible for transferring significant amounts of energy across the wavenumber spectrum and provided significant insight into the mechanics of the evolution of surface-gravity waves.

Phillips' work, and a large number of follow-up papers, such as the work of Longuet-Higgins (1962), apply a regular perturbation scheme to determine modal

growth rates and quantify the rate of energy transfer among interacting waves. However, the time range over which this scheme is applicable is steepness limited. Subsequent work by Benney (1962) and McGoldrick (1965) applied the method of multiple scales to extend the theory of resonant wave–wave interactions by developing coupled nonlinear interaction equations for a discrete set of resonant wave modes. McGoldrick derived closed-form solutions in terms of Jacobi elliptic functions, which described the interfacial elevation of these discrete modes and demonstrated energy conservation (for non-dissipative conditions). This multiscale expansion was demonstrated to be accurate for times up to an order of magnitude longer than the traditional regular perturbation scheme. Since Phillips' (1960) paper, the theory of resonant wave–wave interactions among surface gravity waves has been a subject of active research and has reached maturity.

Janssen (1986) and Janssen (1987) considered the effects of resonant interactions between a primary wave and its second harmonic (referred to as a second harmonic resonance or an overtone resonance). His work found that this class of resonant interactions is responsible for the observed period doubling behaviour seen in spectral measurements. More recently, Bontozoglou & Hanratty (1990) speculated that finite-amplitude Kelvin–Helmholtz waves undergo an internal second harmonic resonance which would result in the doubling of the wavelength of the unstable wave. It was believed that this could be part of the initial mechanism which would lead to the formation of slugs.

Recently Romanova & Annenkov (2005) studied three-wave resonant interactions in a multilayer stratified flow using a Hamiltonian formulation. They derived a set of coupled nonlinear interaction equations for the evolution of a resonant triad with one interacting wave component being linearly unstable. They found that the resonant interaction with stable waves can stabilize the growth of the linearly unstable wave. Similar work was also carried out in the study of baroclinic wave dynamics based on a quasi-geostrophic two-layer model by Loesch (1974), Pedlosky (1975) and Mansbridge & Smith (1983). All of these studies did not focus on the growth of stable waves in the resonance. In addition, the influence of the zeroth harmonic (resulted from quadratic self-interactions in finite depth) on the evolution of the interacting waves was not accounted for.

In this work, we study theoretically and computationally the effects of nonlinear resonant wave interactions coupled with interfacial instability upon the development of long waves on the interface of a two-fluid stratified flow. We consider a two-dimensional canonical problem of triad interfacial wave resonance involving one unstable short wave, which is linearly unstable due to the Kelvin–Helmholtz mechanism, and two stable waves in a two-layer stratified horizontal channel flow. Based on the observation of slug flow experiments, it is of interest to have one of the stable waves in the resonant triad with a wavelength much larger than that of the unstable wave. Since our focus is on the understanding of the nonlinear mechanism for energy transfer from short unstable waves to long stable waves, we assume simple uniform base flows for the two fluids and formulate the problem in the context of potential flow (§ 2.1). We derive the evolution equations for the amplitudes of the interacting waves, including both interfacial instability and resonant wave interaction effects, by the use of the method of multiple scales (§ 2.4). Based on the evolution equations, we analyse the characteristic features of triad resonance and nonlinear interfacial instability. Of particular interest is that under certain flow conditions, there exists a strong mechanism for effectively transferring energy from (unstable) short waves to (stable) long waves (§ 2.5). For validation of the theory and application

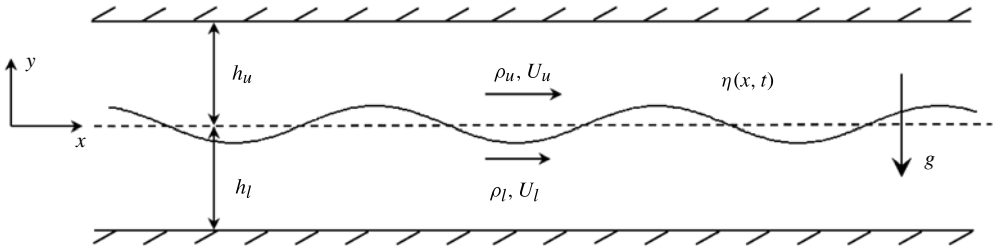

FIGURE 1. Definition sketch of a two-layer stratified flow in a horizontal channel.

to realistic situations involving multiple resonances, an effective numerical method based on the high-order pseudo-spectral approach is developed (§ 3). The theory and numerical simulation are cross-validated for the characteristic cases presented. Moreover, the trends observed in the direct simulation agree qualitatively with the experimental measurement of initial slug time/length for a two-layer flow entering into a horizontal pipe (§ 4). This work provides an insight into the basic nonlinear physics that may play a significant role in the initial development of slugs in stratified channel/pipe flows.

2. Theoretical analysis

This analysis considers the nonlinear evolution of interfacial waves propagating through a stratified two-fluid horizontal channel. It is of fundamental interest to understand the characteristic features of wave energy transfer associated with triad resonant interaction, particularly when one of the wave components in the triad is linearly unstable to the Kelvin–Helmholtz mechanism.

2.1. *Fully nonlinear governing equations*

A fixed Cartesian coordinate system is established with the origin located at the undisturbed interface between the two fluids with the x-axis extending horizontally to the right and the y-axis being directed vertically upwards. The fluids have equilibrium depths of h_u and h_l with the upper and lower fluids being denoted by the subscripts u and l, respectively. The vertical displacement of the interface away from its undisturbed position is defined by the function $y = \eta\,(x, t)$. The two fluids, which are assumed to be immiscible, are of density ρ_u and ρ_l, with $\rho_u < \rho_l$. The effects of gravity g and surface tension γ are also taken into account. A sketch of the problem is illustrated in figure 1.

The flow in each domain is decomposed into a constant uniform current (U_u and U_l) and a disturbance flow. It is assumed that both flows are incompressible and irrotational such that the velocity of each fluid is defined by the gradient of its potential function, $\varphi_u\,(x, y, t) = U_u x + \phi_u(x, y, t)$ and $\varphi_l\,(x, y, t) = U_l x + \phi_l(x, y, t)$. The disturbance potentials (ϕ_u and ϕ_l) must satisfy Laplace's equation in the fluid domain:

$$\nabla^2\phi_u = 0, \quad \eta < y < h_u \tag{2.1}$$

$$\nabla^2\phi_l = 0, \quad -h_l < y < \eta. \tag{2.2}$$

At the channel walls, the no flux conditions are enforced as

$$\phi_{u,y} = 0, \quad y = h_u \tag{2.3}$$

$$\phi_{l,y} = 0, \quad y = -h_l. \tag{2.4}$$

Requiring that the interface remain material produces

$$\eta_{,t} + (U_u + \phi_{u,x})\eta_{,x} = \phi_{u,y}, \quad y = \eta \tag{2.5}$$

$$\eta_{,t} + (U_l + \phi_{l,x})\eta_{,x} = \phi_{l,y}, \quad y = \eta \tag{2.6}$$

while the balance of normal stresses at the interface between the two fluids gives

$$\mathscr{R}\left[\phi_{u,t} + \frac{1}{2}(\nabla\phi_u)^2 + U_u\phi_{u,x} + \eta\right] - \left[\phi_{l,t} + \frac{1}{2}(\nabla\phi_l)^2 + U_l\phi_{l,x} + \eta\right]$$
$$= -\frac{\eta_{,xx}}{\mathscr{W}}(1 + \eta_{,x}^2)^{-3/2}, \quad y = \eta \tag{2.7}$$

where $\mathscr{R} \equiv \rho_u/\rho_l$ is the density ratio and $\mathscr{W} \equiv \mathscr{L}^2 g\rho_l/\gamma$ is the Weber number. In the above equations, the quantities are non-dimensionalized in terms of the characteristic length $\mathscr{L}$ and time $\mathscr{T} = (\mathscr{L}/g)^{1/2}$. This problem is complete with the specification of an appropriate set of initial conditions for ϕ_u, ϕ_l and η.

2.2. *Linear theory and the Kelvin–Helmholtz instability*

For the purpose of better understanding the nonlinear analysis in the following sections, it is beneficial to review the key findings from the classical linear theory. The linearization of (2.1)–(2.7) in terms of the small interfacial wave steepness ϵ produces

$$\nabla^2\phi_u = 0, \quad 0 < y < h_u \tag{2.8a}$$

$$\nabla^2\phi_l = 0, \quad -h_l < y < 0 \tag{2.8b}$$

$$\phi_{u,y} = 0, \quad y = h_u \tag{2.8c}$$

$$\phi_{l,y} = 0, \quad y = -h_l \tag{2.8d}$$

$$\eta_{,t} + U_u\eta_{,x} - \phi_{u,y} = 0, \quad y = 0 \tag{2.8e}$$

$$\eta_{,t} + U_l\eta_{,x} - \phi_{l,y} = 0, \quad y = 0 \tag{2.8f}$$

$$\mathscr{R}(\phi_{u,t} + U_u\phi_{u,x} + \eta) - (\phi_{l,t} + U_l\phi_{l,x} + \eta) + \frac{\eta_{,xx}}{\mathscr{W}} = 0, \quad y = 0. \tag{2.8g}$$

A travelling wave solution of (2.8) takes the form

$$\eta = \frac{\eta_o}{2}\mathrm{e}^{\mathrm{i}(kx-\omega t)} + \text{c.c.} \tag{2.9a}$$

$$\phi_u = \eta_o \frac{-\mathrm{i}(U_u k - \omega)}{2k\tanh kh_u}\frac{\cosh k(y - h_u)}{\cosh kh_u}\mathrm{e}^{\mathrm{i}(kx-\omega t)} + \text{c.c.} \tag{2.9b}$$

$$\phi_l = \eta_o \frac{\mathrm{i}(U_l k - \omega)}{2k\tanh kh_l}\frac{\cosh k(y + h_l)}{\cosh kh_l}\mathrm{e}^{\mathrm{i}(kx-\omega t)} + \text{c.c.} \tag{2.9c}$$

where η_o is the amplitude of the (initial) wave disturbance, k is the wavenumber and ω is the frequency. The symbol 'c.c.' represents the complex conjugate of the preceding

term(s). The frequency ω is related to the wavenumber k by the dispersion relation:

$$\omega = \frac{k(U_u\mathscr{R}T_l + U_lT_u)}{\mathscr{R}T_l + T_u} \pm k\left[\frac{1}{k}\left(\frac{T_uT_l}{\mathscr{R}T_l + T_u}\right)\right.$$
$$\left.\times\left(1 - \mathscr{R} + \frac{k^2}{\mathscr{W}}\right) - \frac{\mathscr{R}\,(U_u - U_l)^2\,T_uT_l}{(\mathscr{R}T_l + T_u)^2}\right]^{1/2} \tag{2.10}$$

where $T_{u/l} \equiv \tanh kh_{u/l}$. From (2.10), it is clear that ω is a complex number if $|U_u - U_l| > U_c$ with the critical velocity U_c defined as

$$U_c(k) \equiv \left[\frac{(\mathscr{R}T_l + T_u)}{\mathscr{R}k}\left(1 - \mathscr{R} + \frac{k^2}{\mathscr{W}}\right)\right]^{1/2}. \tag{2.11}$$

Under this condition, the wave (of wavenumber k) is unstable with its amplitude growing exponentially with time by drawing energy from base flows.

Without loss of generality, we assume that $U_u > U_l$ in the following analysis and we consider the case with $U_u - U_l$ slightly exceeding U_c, i.e. $U_u - U_l = U_c(1 + \Delta)$ where $0 < \Delta \ll 1$. In this case, the frequency can be written as

$$\omega \equiv \omega_R + \mathrm{i}\omega_I$$
$$= \frac{k(U_u\mathscr{R}T_l + U_lT_u)}{\mathscr{R}T_l + T_u} \pm \mathrm{i}\left[\frac{2kT_uT_l}{\mathscr{R}T_l + T_u}\left(1 - \mathscr{R} + \frac{k^2}{\mathscr{W}}\right)\right]^{1/2}\Delta^{1/2} + O(\Delta^{3/2}). \tag{2.12}$$

Clearly, the growth rate $\omega_I = O(\Delta^{1/2})$ while $U_u - U_l - U_c = O(\Delta)$.

2.3. *Triad resonant wave–wave interaction*

In the context of linear theory, waves of different wavelengths (or frequencies) travel independently in time/space. When nonlinear interactions among them are accounted for, locked waves are generated. The amplitudes of the locked waves are generally of higher-order compared with the primary waves. If the frequency and wavenumber of the locked wave satisfy the dispersion relation (2.10), the locked wave becomes a free wave. In this case, the interaction becomes resonant. As a result, the generated free wave can grow significantly with its amplitude being comparable to that of the primary waves. Resonant interactions are known to play a critical role in the evolution of nonlinear ocean surface waves as they cause energy transfer among different wave components in the wave spectrum (e.g. Phillips 1960).

In this study, we consider a triad resonant interaction in which one of the primary waves is unstable due to the Kelvin–Helmholtz effect. The focus is on the mechanism of energy transfer from the unstable wave to the stable waves in the triad. For definiteness, we consider a triad consisting of three free waves with wavenumbers k_1, k_2 and k_3. Without loss of generality, we let $k_3 < k_1 < k_2$ with the k_2 wave being unstable (and k_1 and k_3 waves being stable). Unlike in the conservative wave system in which the frequencies of interacting waves involved are all real, the frequency of the unstable k_2 wave is complex in the present case. The multiple-scale analysis commonly used in the conservative wave system cannot be directly applied here. The evolution of the amplitudes of interacting waves in the triad is now affected not only by the resonant interaction but also by the interfacial instability. The time scales of these two processes need to be properly considered in the analysis. To obtain a basic understanding of the interaction mechanism of these two processes, we consider the k_2 wave to be slightly unstable with $U_u - U_l = U_c(1 + \Delta)$, $\Delta \ll 1$. In the present analysis, we choose to expand the interaction problem at $U_u - U_l = U_c(1 + \Delta)$ with respect to

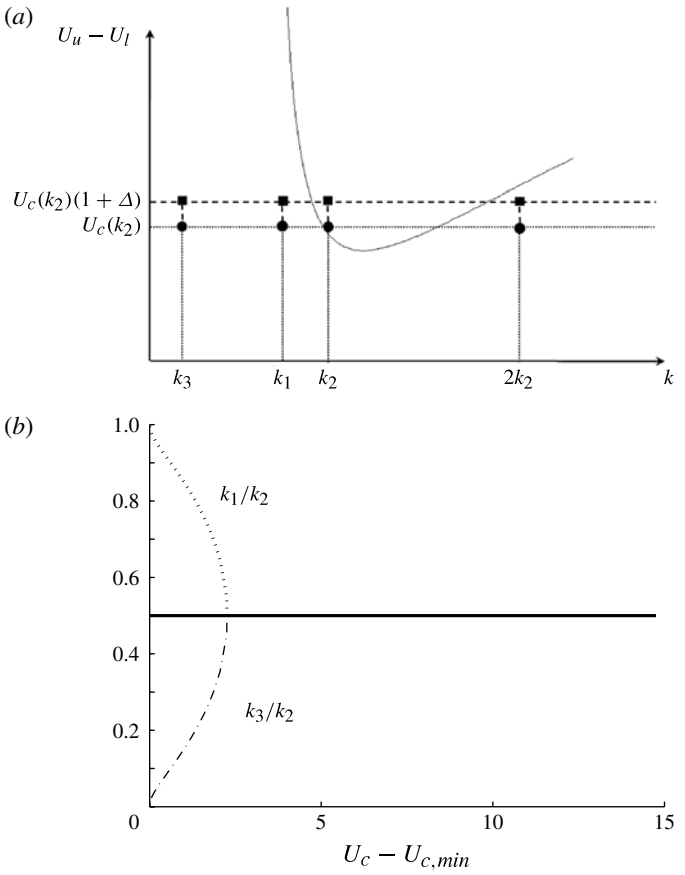

FIGURE 2. (*a*) Sketch of the neutral stability curve (——) and wavenumbers of the primary waves forming a resonant triad (k_1, k_2, k_3) along with the second harmonic ($2k_2$) of the k_2 wave. (*b*) Normalized wavenumbers k_1/k_2 (· · ·) and k_3/k_2 (— · —) in a resonant triad as a function of the critical velocity $U_c(k_2)$. The curve (——) in (*b*) represents the subharmonic resonance with $k_1/k_2 = k_3/k_2 = 0.5$. The results are obtained with $\mathscr{R} = 1.23 \times 10^{-3}$, $\mathscr{W} \cong 845.5$, $H = 1.25$, $\alpha \equiv h_u/H = 0.5$ and $U_l = 1.13$. (With $\mathscr{L} \cong 0.08$ m and $\mathscr{T} \cong 0.09$ s, as an example, these parameters correspond to an air–water flow in a horizontal channel with fixed $h_u = h_l = 0.05$ m, $U_l = 1.0$ m s^{-1} and $\gamma = 0.073$ N m^{-1}.)

the marginally stable state at $U_u - U_l = U_c$ in terms of Δ (Loesch 1974). A sketch of the interacting waves in the plane formed by wavenumber and velocity jump is illustrated in figure 2(*a*).

At the marginally stable state, the k_2 wave is neutrally stable. Following the analysis of Phillips (1960) for conservative resonances, a resonant triad involving k_1, k_2 and k_3 waves are formed under the condition: $k_2 - k_1 = k_3$ and $\omega_2 - \omega_1 = \omega_3$, where $\omega_1(k_1)$ and $\omega_3(k_3)$ are given by (2.10) while for a given k_2, the frequency, $\omega_2(k_2)$, is given by the real part of (2.12). Figure 2(*b*) shows a typical result of k_1 and k_3 (normalized by k_2) as a function of $U_c(k_2)$. The result shown corresponds to the left branch of the neutral stability curve in figure 2(*a*). For lower U_c, the triad resonance involving long and short waves exist. There also exists a subharmonic resonance between k_2 and its subharmonic $k_1 = k_3 = 1/2k_2$. For larger U_c, the triad resonance converges to its

special case of subharmonic resonance. In this work, the analysis is focused on the case of general triad resonance with $k_1 \neq k_3$ (at relatively lower U_c). The subharmonic resonance is to be analysed in a separate study.

In the following analysis, for generality, we consider a near-resonance triad in which the wavenumbers and frequencies of the interacting waves have the relations

$$\begin{cases} k_2 - k_1 = k_3 \\ \omega_2 - \omega_1 = \omega_3 + \sigma \end{cases} \tag{2.13}$$

where σ (with $\sigma \ll \omega_j$, $j = 1, 2, 3$) represents the frequency detuning. Note that the triad resonance condition is satisfied exactly when $\sigma = 0$. In addition, for both simplicity and clarity, the second harmonic of the k_2 wave is assumed to be stable. When this constraint is relived, the analysis procedure is similar, but a different combination in the order of magnitudes of the interacting waves needs to be considered.

2.4. *Multiple-scale analysis*

In this section we shall derive the analytic equations governing the time evolution of the amplitudes of the interacting waves in the triad by use of the method of multiple scales which captures the combined effect of the nonlinear Kelvin–Helmholtz instability and resonant wave–wave interaction.

2.4.1. *Perturbation expansions*

As (2.12) indicates, the growth rate of the k_2 wave is of $O(\Delta^{1/2})$. Thus, there exists two distinct time scales. One is the fast time t associated with the rapid change of the phases of the waves. The other is the slow time τ associated with the time variation of the amplitudes of the waves. Clearly, we have $\tau = \Delta^{1/2}t$ for the present problem. For the perturbation analysis, we assume that the steepness of the interface is small with $O(\epsilon) = O(\Delta^{1/2})$. For convenience, we expand the velocity potentials (ϕ_u and ϕ_l) as well as the interfacial displacement η in a regular perturbation expansion of the form

$$\phi_u(x, y, t, \tau) = \sum_{m=1}^{5} \Delta^{(m+1)/4} \phi_u^{(m)}(x, y, t, \tau) + O(\Delta^{7/4}) \tag{2.14a}$$

$$\phi_l(x, y, t, \tau) = \sum_{m=1}^{5} \Delta^{(m+1)/4} \phi_l^{(m)}(x, y, t, \tau) + O(\Delta^{7/4}) \tag{2.14b}$$

$$\eta(x, t, \tau) = \sum_{m=1}^{5} \Delta^{(m+1)/4} \eta^{(m)}(x, t, \tau) + O(\Delta^{7/4}) \tag{2.14c}$$

where $\phi_u^{(m)}$, $\phi_l^{(m)}$ and $\eta^{(m)}$, $m = 1, \ldots, 5$, are $O(1)$. This expansion is established under the assumption that the amplitude of the unstable wave (k_2) is $O(\Delta^{1/2})$ while that of the other two stable waves (k_1, k_3) are $O(\Delta^{3/4})$. With this order arrangement, the effect of the cubic self-interaction on the evolution of the k_2 wave could be comparable to that of the quadratic (resonant) interactions of the k_1 and k_3 waves. Following the standard procedure of the multiple-scale perturbation analysis, the nonlinear boundary-value problem for ϕ_u and ϕ_l is decomposed into a sequence of linearized boundary-value problems for $\phi_u^{(m)}$ and $\phi_l^{(m)}$, $m = 1, 2, \ldots, 5$, which are presented in Appendix. These problems are then solved sequentially starting from $m = 1$.

2.4.2. *The $O(\Delta^{1/2})$ solution*

At this order, the boundary-value problem is identical to that outlined in § 2.2. The solution for the linearly unstable k_2 wave is

$$\phi_u^{(1)} = \frac{\cosh k_2(y-h_u)}{\cosh k_2 h_u}[\mathscr{P}_2(\tau)\mathrm{e}^{\mathrm{i}\psi_2} + \text{c.c.}] + \phi_{u0}^{(1)}(\tau) \tag{2.15a}$$

$$\phi_l^{(1)} = \frac{\cosh k_2(y+h_l)}{\cosh k_2 h_l}[\mathscr{Q}_2(\tau)\mathrm{e}^{\mathrm{i}\psi_2} + \text{c.c.}] + \phi_{l0}^{(1)}(\tau) \tag{2.15b}$$

$$\eta^{(1)} = \frac{A_2(\tau)}{2}\mathrm{e}^{\mathrm{i}\psi_2} + \text{c.c.} \tag{2.15c}$$

where $\mathscr{P}_2$, $\mathscr{Q}_2$ and ψ_2 are given from the general expressions:

$$\mathscr{P}_j(\tau) = \frac{-\mathrm{i}\mathbb{D}_{uj}A_j(\tau)}{2k_j \tanh k_j h_u}, \quad \mathscr{Q}_j(\tau) = \frac{\mathrm{i}\mathbb{D}_{lj}A_j(\tau)}{2k_j \tanh k_j h_l}, \quad \psi_j = k_j x - \omega_j t \tag{2.16}$$

and $\mathbb{D}_{uj} \equiv (U_l + U_c)k_j - \omega_j$ and $\mathbb{D}_{lj} \equiv U_l k_j - \omega_j$ with the subscript $j = 2$. Note that the boundary-value problem for $\phi_u^{(1)}$ and $\phi_l^{(1)}$ admits space-independent solutions $\phi_{u0}^{(1)}(\tau)$ and $\phi_{l0}^{(1)}(\tau)$ which will be shown to be important in the higher-order solutions. The slow-time dependent amplitude, $A_2(\tau)$, and potentials, $\phi_{u0}^{(1)}(\tau)$ and $\phi_{l0}^{(1)}(\tau)$, are governed by the evolution equations to be developed below.

2.4.3. *The $O(\Delta^{3/4})$ solution*

At this order, the solution represents the (stable) k_1 and k_3 waves:

$$\begin{aligned}\phi_u^{(2)} = {} & \frac{\cosh k_1(y-h_u)}{\cosh k_1 h_u}[\mathscr{P}_1(\tau)\mathrm{e}^{\mathrm{i}\psi_1} + \text{c.c.}] \\ & + \frac{\cosh k_3(y-h_u)}{\cosh k_3 h_u}[\mathscr{P}_3(\tau)\mathrm{e}^{\mathrm{i}\psi_3} + \text{c.c.}] + \phi_{u0}^{(2)}(\tau)\end{aligned} \tag{2.17a}$$

$$\begin{aligned}\phi_l^{(2)} = {} & \frac{\cosh k_1(y+h_l)}{\cosh k_1 h_l}[\mathscr{Q}_1(\tau)\mathrm{e}^{\mathrm{i}\psi_1} \\ & + \text{c.c.}] + \frac{\cosh k_3(y+h_l)}{\cosh k_3 h_l}[\mathscr{Q}_3(\tau)\mathrm{e}^{\mathrm{i}\psi_3} + \text{c.c.}] + \phi_{l0}^{(2)}(\tau)\end{aligned} \tag{2.17b}$$

$$\eta^{(2)} = \frac{A_1(\tau)}{2}\mathrm{e}^{\mathrm{i}\psi_1} + \frac{A_3(\tau)}{2}\mathrm{e}^{\mathrm{i}\psi_3} + \text{c.c.} \tag{2.17c}$$

where $\mathscr{P}_{1,3}$, $\mathscr{Q}_{1,3}$ and $\psi_{1,3}$ are given from the general expressions (2.16) with the subscript $j = 1$ and 3, respectively. Like the $m = 1$ problem, the boundary-value problem at $m = 2$ also admits space-independent potentials, $\phi_{u0}^{(2)}(\tau)$ and $\phi_{l0}^{(2)}(\tau)$, which are functions of slow time. The slow-time-dependent amplitudes, $A_1(\tau)$ and $A_3(\tau)$, are governed by the evolution equations to be developed below.

2.4.4. *The $O(\Delta)$ solution*

The inhomogeneous forcing terms at this order are

$$f_1^{(3)} = -\tfrac{1}{2}\dot{A}_2\mathrm{e}^{\mathrm{i}\psi_2} + p_4 A_2^2\mathrm{e}^{2\mathrm{i}\psi_2} + \text{c.c.} \tag{2.18a}$$

$$f_2^{(3)} = -\tfrac{1}{2}\dot{A}_2\mathrm{e}^{\mathrm{i}\psi_2} + d_4 A_2^2\mathrm{e}^{2\mathrm{i}\psi_2} + \text{c.c.} \tag{2.18b}$$

$$f_3^{(3)} = f_2\dot{A}_2\mathrm{e}^{\mathrm{i}\psi_2} + f_7 A_2^2\mathrm{e}^{2\mathrm{i}\psi_2} + \text{c.c.} + f_8|A_2|^2 + \dot{\phi}_{l0}^{(1)} - \mathscr{R}\dot{\phi}_{u0}^{(1)} \tag{2.18c}$$

with the coefficients given by

$$p_4 = -\frac{1}{2}\mathrm{i}k_2\mathbb{D}_{u2}C_{u2}, \quad d_4 = \frac{1}{2}\mathrm{i}k_2\mathbb{D}_{l2}C_{l2}, \tag{2.19a}$$

$$f_2 = \frac{\mathrm{i}}{2k_2}(\mathbb{D}_{l2}C_{l2} + \mathscr{R}\mathbb{D}_{u2}C_{u2}), \quad f_7 = -\frac{1}{8}[(3 - C_{l2}^2)\mathbb{D}_{l2}^2 - \mathscr{R}(3 - C_{u2}^2)\mathbb{D}_{u2}^2], \tag{2.19b}$$

$$f_8 = \frac{1}{4}[(C_{l2}^2 - 1)\mathbb{D}_{l2}^2 - \mathscr{R}(C_{u2}^2 - 1)\mathbb{D}_{u2}^2] \tag{2.19c}$$

where $C_{u/lj} \equiv \coth(k_j h_{u/l})$ and the symbol '$\cdot$' denotes the derivative with respect to slow time τ. There are zeroth, first and second harmonics in the forcing terms. The boundary-value solution associated with the zeroth and second harmonic forcing can be obtained directly. Since the first harmonic is the homogeneous solution of the boundary-value problem, the first harmonic forcing must satisfy the solvability condition, specified by the Fredholm alternative, in order to obtain a non-trivial inhomogeneous solution. By applying Green's theorem between the $O(\Delta^{1/2})$ and $O(\Delta)$ solutions (for the first harmonic), the solvability condition is found to take the form

$$\frac{\mathrm{i}\dot{A}_2}{k_2}\left[\frac{\mathscr{R}\mathbb{D}_{u2}}{T_{u2}} + \frac{\mathbb{D}_{l2}}{T_{l2}}\right] = G_2\left[\frac{\mathscr{R}\mathbb{D}_{u2}^2}{k_2 T_{u2}} + \frac{\mathbb{D}_{l2}^2}{k_2 T_{l2}} - 1 + \mathscr{R} - \frac{k_2^2}{\mathscr{W}}\right] \tag{2.20}$$

where $T_{u/lj} \equiv \tanh(k_j h_{u/l})$ and G_2 denotes the half amplitude of the first harmonic (propagating wave) of $\eta^{(3)}$. Since k_2 and ω_2 satisfy the dispersion relation, it is straightforward to show that the terms in the brackets on both sides of (2.20) are identically zero. Since all of the structure of the propagating k_2 wave is contained in the $O(\Delta^{1/2})$ solution, G_2 can be set to zero without any loss of generality. The total solution for $\phi_u^{(3)}$, $\phi_l^{(3)}$, and $\eta^{(3)}$ are then written as

$$\phi_u^{(3)} = \frac{\cosh k_2(y - h_u)}{\cosh k_2 h_u}(\alpha_2\dot{A}_2\mathrm{e}^{\mathrm{i}\psi_2} + \text{c.c.}) + \frac{\cosh 2k_2(y - h_u)}{\cosh 2k_2 h_u}(\alpha_{22}A_2^2\mathrm{e}^{2\mathrm{i}\psi_2} + \text{c.c.}) \tag{2.21a}$$

$$\phi_l^{(3)} = \frac{\cosh k_2(y + h_l)}{\cosh k_2 h_l}(\beta_2\dot{A}_2\mathrm{e}^{\mathrm{i}\psi_2} + \text{c.c.}) + \frac{\cosh 2k_2(y + h_l)}{\cosh 2k_2 h_l}(\beta_{22}A_2^2\mathrm{e}^{2\mathrm{i}\psi_2} + \text{c.c.}) \tag{2.21b}$$

$$\eta^{(3)} = \nu_{22}(A_2^2\mathrm{e}^{\mathrm{i}2\psi_2} + \text{c.c.}) + \nu_0|A_2|^2 + \frac{\dot{\phi}_{l0} - \mathscr{R}\dot{\phi}_{u0}}{\mathscr{R} - 1} \tag{2.21c}$$

where

$$\nu_{22} = k_2\frac{\mathbb{D}_{l2}^2\left[2C_{l4}C_{l2} - \frac{1}{2}(3 - C_{l2}^2)\right] - \mathscr{R}\mathbb{D}_{u2}^2\left[2C_{u4}C_{u2} - \frac{1}{2}(3 - C_{u2}^2)\right]}{8\mathscr{R}C_{u4}\mathbb{D}_{u2}^2 + 8C_{l4}\mathbb{D}_{l2}^2 + 4k_2(\mathscr{R} - 1 - (4k_2^2/\mathscr{W}))} \tag{2.22a}$$

$$\nu_0 = \frac{(C_{l2}^2 - 1)\mathbb{D}_{l2}^2 - \mathscr{R}(C_{u2}^2 - 1)\mathbb{D}_{u2}^2}{4(\mathscr{R} - 1)} \tag{2.22b}$$

$$\alpha_2 = -\frac{1}{2k_2 T_{u2}}, \quad \alpha_{22} = -\mathrm{i}\mathbb{D}_{u2}\left(\frac{k_2 C_{u2} + 4\nu_{22}}{4k_2 T_{u4}}\right) \tag{2.22c}$$

$$\beta_2 = \frac{1}{2k_2 T_{l2}}, \quad \beta_{22} = -\mathrm{i}\mathbb{D}_{l2}\left(\frac{k_2 C_{l2} - 4\nu_{22}}{4k_2 T_{l4}}\right) \tag{2.22d}$$

with $C_{u/l4} = \coth(2k_2 h_{u/l})$ and $T_{u/l4} = \tanh(2k_2 h_{u/l})$.

One notes that if the two stable waves (k_1 and k_3) are set to be of $O(\Delta^{1/2})$ like the unstable wave (k_2), an unbalanced resonant interaction term would be present in (2.20).

By letting the two stable waves be $O(\Delta^{1/4})$ smaller than the unstable k_2 wave, the effects of triad resonant interaction and nonlinear Kelvin–Helmholtz instability will converge together correctly in the $O(\Delta^{3/2})$ problem without the presence of singularities in the lower-order solution.

2.4.5. *The $O(\Delta^{5/4})$ solution*

At this order, the only terms in $f_j^{(4)}$ $(j = 1, 2, 3)$ which produce secular terms are those with phase ψ_1 and ψ_3. Upon neglecting the non-secular terms, $f_j^{(4)}$, $j = 1, 2$ and 3, takes the form

$$f_1^{(4)} = -\tfrac{1}{2}\dot{A}_1 e^{i\psi_1} - \tfrac{1}{2}\dot{A}_3 e^{i\psi_3} + p_1 A_1^* A_2 e^{i(\psi_2-\psi_1)} + p_3 A_2 A_3^* e^{i(\psi_2-\psi_3)} + \text{c.c.} \quad (2.23a)$$

$$f_2^{(4)} = -\tfrac{1}{2}\dot{A}_1 e^{i\psi_1} - \tfrac{1}{2}\dot{A}_3 e^{i\psi_3} + d_1 A_1^* A_2 e^{i(\psi_2-\psi_1)} + d_3 A_2 A_3^* e^{i(\psi_2-\psi_3)} + \text{c.c.} \quad (2.23b)$$

$$f_3^{(4)} = f_1\dot{A}_1 e^{i\psi_1} + f_3\dot{A}_3 e^{i\psi_3} + f_4 A_1^* A_2 e^{i(\psi_2-\psi_1)} + f_6 A_2 A_3^* e^{i(\psi_2-\psi_3)} + \text{c.c.} + \dot{\phi}_{l0}^{(2)} - \mathscr{R}\dot{\phi}_{u0}^{(2)} \quad (2.23c)$$

where $\psi_2 - \psi_1 = \psi_3 - \varpi\tau$ and $\psi_2 - \psi_3 = \psi_1 - \varpi\tau$ with $\varpi = \sigma\Delta^{-1/2}$, and the coefficients are given by

$$p_1 = -\frac{1}{4}ik_3(\mathbb{D}_{u1}C_{u1} + \mathbb{D}_{u2}C_{u2}), \quad p_3 = -\frac{1}{4}ik_1(\mathbb{D}_{u2}C_{u2} + \mathbb{D}_{u3}C_{u3}) \quad (2.24a)$$

$$d_1 = \frac{1}{4}ik_3(\mathbb{D}_{l1}C_{l1} + \mathbb{D}_{l2}C_{l2}), \quad d_3 = \frac{1}{4}ik_1(\mathbb{D}_{l2}C_{l2} + \mathbb{D}_{l3}C_{l3}) \quad (2.24b)$$

$$f_1 = \frac{i}{2k_1}(\mathbb{D}_{l1}C_{l1} + \mathscr{R}\mathbb{D}_{u1}C_{u1}), \quad f_3 = \frac{i}{2k_3}(\mathbb{D}_{l3}C_{l3} + \mathscr{R}\mathbb{D}_{u3}C_{u3}) \quad (2.24c)$$

$$f_4 = \frac{1}{4}\{\mathscr{R}[\mathbb{D}_{u1}^2 + \mathbb{D}_{u2}^2 - (1 + C_{u1}C_{u2})\mathbb{D}_{u1}\mathbb{D}_{u2}] - \mathbb{D}_{l1}^2 - \mathbb{D}_{l2}^2 + (1 + C_{l1}C_{l2})\mathbb{D}_{l1}\mathbb{D}_{l2}\} \quad (2.24d)$$

$$f_6 = \frac{1}{4}\{\mathscr{R}[\mathbb{D}_{u2}^2 + \mathbb{D}_{u3}^2 - (1 + C_{u2}C_{u3})\mathbb{D}_{u2}\mathbb{D}_{u3}] - \mathbb{D}_{l2}^2 - \mathbb{D}_{l3}^2 + (1 + C_{l2}C_{l3})\mathbb{D}_{l2}\mathbb{D}_{l3}\}. \quad (2.24e)$$

Upon the use of the solvability conditions which can be realized by applying Green's theorem to the $O(\Delta^{3/4})$ and $O(\Delta^{5/4})$ solutions, we obtain the evolution equations for A_1 and A_3:

$$\dot{A}_1 = iB_{23}A_2A_3^* e^{-i\varpi\tau} \quad (2.25a)$$

$$\dot{A}_3 = iB_{12}A_1^* A_2 e^{-i\varpi\tau} \quad (2.25b)$$

where

$$B_{23} = \frac{k_1}{4}\left[\frac{\mathbb{D}_{l1}C_{l1}(\mathbb{D}_{l2}C_{l2} + \mathbb{D}_{l3}C_{l3}) - \mathbb{D}_{l2}^2 - \mathbb{D}_{l3}^2 + (1 + C_{l2}C_{l3})\mathbb{D}_{l2}\mathbb{D}_{l3}}{\mathscr{R}\mathbb{D}_{u1}C_{u1} + \mathbb{D}_{l1}C_{l1}}\right] - \frac{\mathscr{R}k_1}{4}\left[\frac{\mathbb{D}_{u1}C_{u1}(\mathbb{D}_{u2}C_{u2} + \mathbb{D}_{u3}C_{u3}) - \mathbb{D}_{u2}^2 - \mathbb{D}_{u3}^2 + (1 + C_{u2}C_{u3})\mathbb{D}_{u2}\mathbb{D}_{u3}}{\mathscr{R}\mathbb{D}_{u1}C_{u1} + \mathbb{D}_{l1}C_{l1}}\right] \quad (2.26a)$$

$$B_{12} = \frac{k_3}{4}\left[\frac{\mathbb{D}_{l3}C_{l3}(\mathbb{D}_{l1}C_{l1} + \mathbb{D}_{l2}C_{l2}) - \mathbb{D}_{l1}^2 - \mathbb{D}_{l2}^2 + (1 + C_{l1}C_{l2})\mathbb{D}_{l1}\mathbb{D}_{l2}}{\mathscr{R}\mathbb{D}_{u3}C_{u3} + \mathbb{D}_{l3}C_{l3}}\right] - \frac{\mathscr{R}k_3}{4}\left[\frac{\mathbb{D}_{u3}C_{u3}(\mathbb{D}_{u1}C_{u1} + \mathbb{D}_{u2}C_{u2}) - \mathbb{D}_{u1}^2 - \mathbb{D}_{u2}^2 + (1 + C_{u1}C_{u2})\mathbb{D}_{u1}\mathbb{D}_{u2}}{\mathscr{R}\mathbb{D}_{u3}C_{u3} + \mathbb{D}_{l3}C_{l3}}\right]. \quad (2.26b)$$

These two interaction coefficients, B_{23} and B_{12}, are the same as those in the case where all three waves in the resonant triad are linearly stable to the Kelvin–Helmholtz effect, as shown by Campbell (2009).

2.4.6. *The $O(\Delta^{3/2})$ solution*

The forcing terms $f_j^{(5)}$, $j = 1$, 2 and 3, are

$$f_1^{(5)} = (p_2 A_1 A_3 \mathrm{e}^{\mathrm{i}\varpi\tau} + p_5 |A_2|^2 A_2 + p_6 A_2(\mathscr{R}\dot{\phi}_{u0}^{(1)} - \dot{\phi}_{l0}^{(1)}) + p_7 A_2 + \text{c.c.})\mathrm{e}^{\mathrm{i}\psi_2} + \frac{\mathscr{R}\ddot{\phi}_{u0}^{(1)} - \ddot{\phi}_{l0}^{(1)}}{\mathscr{R} - 1} - \nu_0 \frac{\mathrm{d}}{\mathrm{d}\tau}(|A_2|^2) \tag{2.27a}$$

$$f_2^{(5)} = (d_2 A_1 A_3 \mathrm{e}^{\mathrm{i}\varpi\tau} + d_5 |A_2|^2 A_2 + d_6 A_2(\mathscr{R}\dot{\phi}_{u0}^{(1)} - \dot{\phi}_{l0}^{(1)}) + \text{c.c.})\mathrm{e}^{\mathrm{i}\psi_2} + \frac{\mathscr{R}\ddot{\phi}_{u0}^{(1)} - \ddot{\phi}_{l0}^{(1)}}{\mathscr{R} - 1} - \nu_0 \frac{\mathrm{d}}{\mathrm{d}\tau}(|A_2|^2) \tag{2.27b}$$

$$f_3^{(5)} = [f_5 A_1 A_3 + f_9 \ddot{A}_2 + f_{10} A_2 + f_{11} |A_2|^2 A_2 + f_{13} A_2(\mathscr{R}\dot{\phi}_{u0}^{(1)} - \dot{\phi}_{l0}^{(1)}) + \text{c.c.}]\mathrm{e}^{\mathrm{i}\psi_2} + f_{12}\dot{A}_2 A_2^* + f_{12}^* \dot{A}_2^* A_2 + f_{14} |A_1|^2 + f_{15} |A_3|^2 \tag{2.27c}$$

where $*$ denotes the complex conjugate and the coefficients are given by

$$p_2 = -\frac{1}{4}\mathrm{i}k_2 (\mathbb{D}_{u1} C_{u1} + \mathbb{D}_{u3} C_{u3}) \tag{2.28a}$$

$$p_5 = \alpha_{22} k_2^2 + \frac{1}{2}\mathrm{i}k_2 \mathbb{D}_{u2} \left[\frac{3}{8}k_2 - C_{u2}(\nu_{22} + \nu_0)\right] \tag{2.28b}$$

$$p_6 = -\frac{ik_2 D_{u2} C_{u2}}{2(\mathscr{R} - 1)} \tag{2.28c}$$

$$p_7 = -\frac{iU_c k_2}{2} \tag{2.28d}$$

$$d_2 = \frac{1}{4}\mathrm{i}k_2 (\mathbb{D}_{l1} C_{l1} + \mathbb{D}_{l3} C_{l3}) \tag{2.28e}$$

$$d_5 = \beta_{22} k_2^2 + \frac{1}{2}\mathrm{i}k_2 \mathbb{D}_{l2} \left[\frac{3}{8}k_2 + C_{l2}(\nu_{22} + \nu_0)\right] \tag{2.28f}$$

$$d_6 = \frac{\mathrm{i}k_2 D_{l2} C_{l2}}{2(\mathscr{R} - 1)} \tag{2.28g}$$

$$f_5 = \frac{1}{4}\left\{(C_{l1} C_{l3} - 1)\mathbb{D}_{l1}\mathbb{D}_{l3} - \mathbb{D}_{l1}^2 - \mathbb{D}_{l3}^2 - \mathscr{R}\left[(C_{u1} C_{u3} - 1)\mathbb{D}_{u1}\mathbb{D}_{u3} - \mathbb{D}_{u1}^2 - \mathbb{D}_{u3}^2\right]\right\} \tag{2.28h}$$

$$f_9 = \beta_2 - \mathscr{R}\alpha_2 \tag{2.28i}$$

$$f_{10} = -\frac{1}{2}\mathscr{R} U_c \mathbb{D}_{u2} C_{u2} \tag{2.28j}$$

$$f_{11} = R\left(\mathrm{i}k_2 \mathbb{D}_{u2}\alpha_{22}[T_{u4} - C_{u2}] + \frac{1}{2}\mathbb{D}_{u2}\left[\nu_0 + \nu_{22} + \frac{5}{8}k_2 C_{u2}\right]\right) - \frac{3k_2^4}{16\mathscr{W}} + \frac{1}{2}\mathbb{D}_{l2}^2\left[\frac{5}{8}k_2 C_{l2} - \nu_0 - \nu_{22}\right] + \mathrm{i}k_2 \mathbb{D}_{l2}\beta_{22}[T_{l4} - C_{l2}] \tag{2.28k}$$

$$f_{12} = \frac{\mathrm{i}}{4}\mathbb{D}_{l2} - \frac{\mathrm{i}}{2}k_2\beta_2 \mathbb{D}_{l2} C_{l2} - \mathscr{R}\left[\frac{\mathrm{i}}{4}\mathbb{D}_{u2} + \frac{\mathrm{i}}{2}k_2\alpha_2 \mathbb{D}_{u2} C_{u2}\right] \tag{2.28l}$$

$$f_{13} = \frac{\mathbb{D}_{l2}^2 - \mathscr{R}\mathbb{D}_{u2}^2}{2(\mathscr{R}-1)} \tag{2.28m}$$

$$f_{14} = \frac{1}{4}\left[D_{l1}^2(C_{l1}^2-1) - \mathscr{R}D_{u1}^2(C_{u1}^2-1)\right] \tag{2.28n}$$

$$f_{15} = \frac{1}{4}\left[D_{l3}^2(C_{l3}^2-1) - \mathscr{R}D_{u3}^2(C_{u3}^2-1)\right]. \tag{2.28o}$$

In (2.27), the non-relevant terms are not included for clarity.

Imposing the solvability condition for the forcing with phase ψ_2, we obtain the evolution equation for A_2:

$$\ddot{A}_2 = \Omega A_2 + \mathscr{N}|A_2|^2 A_2 + \mathscr{M}A_2\left(\mathscr{R}\dot{\phi}_{u0}^{(1)} - \dot{\phi}_{l0}^{(1)}\right) + B_{13}A_1A_3\mathrm{e}^{\mathrm{i}\varpi\tau} \tag{2.29}$$

with

$$\Omega = \frac{-\mathscr{R}U_c\mathbb{D}_{u2}C_{u2}}{\mathscr{R}\alpha_2 - \beta_2} \tag{2.30}$$

$$\begin{aligned}\mathscr{N} = {} & \mathrm{i}k_2\frac{\mathscr{R}\alpha_{22}\mathbb{D}_{u2}[T_{u4}-2C_{u2}] + \beta_{22}\mathbb{D}_{l2}[T_{l4}-2C_{l2}]}{\mathscr{R}\alpha_2-\beta_2} \\ & + \frac{\mathscr{R}\mathbb{D}_{u2}^2[(\nu_0+\nu_{22})(1-C_{u2}^2)+k_2C_{u2}] + \mathbb{D}_{l2}^2[(\nu_0+\nu_{22})(C_{l2}^2-1)+k_2C_{l2}]}{2(\mathscr{R}\alpha_2-\beta_2)} \\ & - \frac{3k_2^4}{16\mathscr{W}(\mathscr{R}\alpha_2-\beta_2)}\end{aligned} \tag{2.31}$$

$$\mathscr{M} = \frac{\mathbb{D}_{l2}^2(1-C_{l2}^2) + \mathscr{R}\mathbb{D}_{u2}^2(C_{u2}^2-1)}{2(\mathscr{R}-1)(\mathscr{R}\alpha_2-\beta_2)} \tag{2.32}$$

$$\begin{aligned}B_{13} = {} & \frac{(C_{l1}C_{l3}-1)\mathbb{D}_{l1}\mathbb{D}_{l3} - \mathbb{D}_{l1}^2 - \mathbb{D}_{l3}^2 - \mathscr{R}[(C_{u1}C_{u3}-1)\mathbb{D}_{u1}\mathbb{D}_{u3} - \mathbb{D}_{u1}^2 - \mathbb{D}_{u3}^2]}{4(\mathscr{R}\alpha_2-\beta_2)} \\ & - \frac{\mathscr{R}\mathbb{D}_{u2}C_{u2}(\mathbb{D}_{u1}C_{u1}+\mathbb{D}_{u3}C_{u3}) - \mathbb{D}_{l2}C_{l2}(\mathbb{D}_{l1}C_{l1}+\mathbb{D}_{l3}C_{l3})}{4(\mathscr{R}\alpha_2-\beta_2)}.\end{aligned} \tag{2.33}$$

Equation (2.29) requires that $\mathscr{R}\dot{\phi}_{u0}^{(1)} - \dot{\phi}_{l0}^{(1)}$ be solved for. For the zeroth harmonic, the boundary-value problem for $\phi_u^{(m)}$ and $\phi_l^{(m)}$ in (A 2*a*)–(A 2*f*) allows for a solution that can be a function of slow time τ only. Thus, the zeroth harmonic forcing in $f_1^{(5)}$ and $f_2^{(5)}$ must vanish, which leads to

$$\mathscr{R}\ddot{\phi}_{u0}^{(1)} - \ddot{\phi}_{l0}^{(1)} = (\mathscr{R}-1)\nu_0\frac{\mathrm{d}}{\mathrm{d}\tau}|A_2|^2. \tag{2.34}$$

Integration of this equation with respect to τ gives

$$\mathscr{R}\dot{\phi}_{u0}^{(1)} - \dot{\phi}_{l0}^{(1)} = (\mathscr{R}-1)\nu_0|A_2|^2 + C \tag{2.35}$$

where the integration constant is determined by the initial condition, $C = \mathscr{R}\dot{\phi}_{u0}^{(1)} - \dot{\phi}_{l0}^{(1)} - (\mathscr{R}-1)\nu_0|A_2|^2$ evaluated at $\tau = 0$.

The leading-order solution of the mean interface elevation in (2.21*c*) then becomes

$$\bar{\eta}^{(3)} = \nu_0|A_2|^2 - \frac{\mathscr{R}\dot{\phi}_{u0}^{(1)} - \dot{\phi}_{l0}^{(1)}}{\mathscr{R}-1} = \frac{C}{1-\mathscr{R}}. \tag{2.36}$$

The zeroth harmonic forcing in $f_3^{(4)}$ and $f_3^{(5)}$ gives the higher-order solution: $\bar{\eta}^{(4)} + \bar{\eta}^{(5)} = [\dot{\phi}_{l0}^{(2)} - \mathscr{R}\dot{\phi}_{u0}^{(2)} + f_{12}\dot{A}_2 A_2^* + f_{12}^* \dot{A}_2^* A_2 + f_{14}\,|A_1|^2 + f_{15}\,|A_3|^2]/(\mathscr{R} - 1)$ where the quantity $\dot{\phi}_{l0}^{(2)} - \mathscr{R}\dot{\phi}_{u0}^{(2)}$ needs to be determined in the $O(\Delta^{7/4})$ boundary-value problem.

Upon substitution of $t = \Delta^{-1/2}\tau$, $a_2 = \Delta^{1/2}A_2$, $a_1 = \Delta^{3/4}A_1$, $a_3 = \Delta^{3/4}A_3$, and $\sigma = \varpi\Delta^{-1/2}$, we rewrite the evolution equations for the amplitudes of the interacting waves in the triad in the form

$$\frac{\mathrm{d}^2 a_2}{\mathrm{d}t^2} = \hat{\Omega} a_2 + \hat{\mathscr{N}}\,|a_2|^2 a_2 + B_{13} a_1 a_3 \mathrm{e}^{\mathrm{i}\sigma t} \tag{2.37a}$$

$$\frac{\mathrm{d}a_1}{\mathrm{d}t} = \mathrm{i}B_{23} a_2 a_3^* \mathrm{e}^{-\mathrm{i}\sigma t} \tag{2.37b}$$

$$\frac{\mathrm{d}a_3}{\mathrm{d}t} = \mathrm{i}B_{12} a_2 a_1^* \mathrm{e}^{-\mathrm{i}\sigma t} \tag{2.37c}$$

where $\hat{\Omega} = (\Omega + \mathscr{M}C)\Delta$ and $\hat{\mathscr{N}} = \mathscr{N} + \mathscr{M}(\mathscr{R} - 1)\nu_0$. In the right-hand side of (2.37*a*), the first term represents the linear Kelvin–Helmholtz instability effect, the second-term the nonlinear correction (associated with cubic self-interactions) to the Kelvin–Helmholtz instability effect and the third term the triad resonant interaction effect. The effect of the mean interface elevation upon the Kelvin–Helmholtz instability is also considered with the inclusion of C in $\hat{\Omega}$.

2.5. *Properties of the nonlinear interaction equations*

The analytic solution to (2.37) is, in general, not known and can only be found through numerical integration. In the case of a perfect resonance ($\sigma = 0$) or for small time, analytical solutions or integral properties can be derived.

2.5.1. *Resonant interactions with* $\sigma = 0$

For the perfect resonance case, $\sigma = 0$. With the decomposition $a_j(t) = R_j(t)\mathrm{e}^{\mathrm{i}\theta_j(t)}$, $j = 1$, 2 and 3, (2.37*b*) and (2.37*c*) are separated into real and imaginary parts:

$$\dot{R}_1 = -B_{23} R_2 R_3 \sin\Phi \tag{2.38a}$$

$$R_1\dot{\theta}_1 = B_{23} R_2 R_3 \cos\Phi \tag{2.38b}$$

$$\dot{R}_3 = -B_{12} R_1 R_2 \sin\Phi \tag{2.38c}$$

$$R_3\dot{\theta}_3 = B_{12} R_1 R_2 \cos\Phi \tag{2.38d}$$

where $\Phi = \theta_2 - \theta_1 - \theta_3$. Using (2.38*a*) and (2.38*c*) and integrating with respect to time, we obtain

$$\mathscr{B}[R_1^2(\tau) - R_1^2(0)] = [R_3^2(\tau) - R_3^2(0)] \tag{2.39}$$

where $\mathscr{B} = B_{12}/B_{23}$. For $\mathscr{B} < 0$, we have from (2.39) that $|\mathscr{B}|R_1^2(t) + R_3^2(t) = |\mathscr{B}|R_1^2(0) + R_3^2(0)$. This indicates that for $\mathscr{B} < 0$, the growth of R_1 and R_3 remains bounded with their maximum amplitudes being limited by their initial conditions. For $\mathscr{B} > 0$, (2.39) shows that there is no restriction on how large the two waves can grow due to the resonant interaction with the unstable k_2 wave.

2.5.2. *Solution at small time*

When the amplitudes of the interacting modes are small (with $k_2 a_2 \ll 1$ and $a_1/a_2, a_3/a_2 \ll 1$), the nonlinear terms in (2.37*a*) have a weak secondary effect. This leaves the evolution equation of a_2 to be dominated by the linear instability. With this simplification, the coupled evolution (2.37) can be solved for the (initial) growth

rates of a_2, a_1 and a_3 due to the linear instability and the triad resonant interaction. Evolution at small initial time (with $a_1/a_2, a_3/a_2 \ll 1$) is an example of this situation.

In this case, it is straightforward to obtain $a_2(t) = \hat{a}_2 \exp\{\hat{\Omega}^{1/2}t\}$ where $\hat{a}_2$ is the initial value of a_2 at $t = 0$. By taking the time derivative of (2.37*c*), we have

$$\ddot{a}_3 = \mathrm{i}B_{12}\left(a_1^*\dot{a}_2 + \dot{a}_1^* a_2 - \mathrm{i}\sigma a_1^* a_2\right)\mathrm{e}^{-\mathrm{i}\sigma t}. \tag{2.40}$$

Upon substitution of $a_2(t)$ and use of (2.37*b*), we rewrite the above equation as

$$\ddot{a}_3 = \left(\sqrt{\hat{\Omega}} - \mathrm{i}\sigma\right)\dot{a}_3 + |\hat{a}_2|^2\, e^{2\sqrt{\hat{\Omega}}t} B_{12}B_{23}a_3. \tag{2.41}$$

Introducing the change of variable $\xi = |\hat{a}_2|\,(B_{12}B_{23})^{1/2}\exp\{\hat{\Omega}^{1/2}t\}$, we write (2.41) in the form

$$\xi^2\frac{\mathrm{d}^2 a_3}{\mathrm{d}\xi^2} + \frac{\mathrm{i}\sigma}{\sqrt{\hat{\Omega}}}\xi\frac{\mathrm{d}a_3}{\mathrm{d}\xi} - \frac{\xi^2}{\hat{\Omega}}a_3 = 0 \tag{2.42}$$

which is a transformed version of the Bessel differential equation. The general solution of (2.42) takes the form

$$a_3(\xi) = \xi^{-\nu}\left[\mathbb{C}_1^{(3)}\mathrm{J}_\nu\left(\frac{-\mathrm{i}\xi}{\sqrt{\hat{\Omega}}}\right) + \mathbb{C}_2^{(3)}\mathrm{Y}_\nu\left(\frac{-\mathrm{i}\xi}{\sqrt{\hat{\Omega}}}\right)\right] \tag{2.43}$$

where $\nu = (\mathrm{i}\sigma - \sqrt{\hat{\Omega}})/(2\sqrt{\hat{\Omega}})$, and J_ν and Y_ν represent the Bessel functions of the first and second kinds, respectively. The constants $\mathbb{C}_1^{(3)}$ and $\mathbb{C}_2^{(3)}$ are determined from the initial condition to be

$$\mathbb{C}_1^{(3)} = \frac{\xi_0^\nu[\hat{a}_3\mathrm{Y}_{\nu+1}(-\mathrm{i}\xi_0/\sqrt{\hat{\Omega}}) + \mathrm{i}\sqrt{\hat{\Omega}}\hat{a}_1^*\hat{a}_2 B_{12}\mathrm{Y}_\nu(-\mathrm{i}\xi_0/\sqrt{\hat{\Omega}})]}{\mathrm{J}_\nu(-\mathrm{i}\xi_0/\sqrt{\hat{\Omega}})\mathrm{Y}_{\nu+1}(-\mathrm{i}\xi_0/\sqrt{\hat{\Omega}}) - \mathrm{J}_{\nu+1}(-\mathrm{i}\xi_0/\sqrt{\hat{\Omega}})\mathrm{Y}_\nu(-\mathrm{i}\xi_0/\sqrt{\hat{\Omega}})} \tag{2.44a}$$

$$\mathbb{C}_2^{(3)} = -\frac{\xi_0^\nu[\hat{a}_3\mathrm{J}_{\nu+1}(-\mathrm{i}\xi_0/\sqrt{\hat{\Omega}}) + \mathrm{i}\sqrt{\hat{\Omega}}\hat{a}_1^*\hat{a}_2 B_{12}\mathrm{J}_\nu(-\mathrm{i}\xi_0/\sqrt{\hat{\Omega}})]}{\mathrm{J}_\nu(-\mathrm{i}\xi_0/\sqrt{\hat{\Omega}})\mathrm{Y}_{\nu+1}(-\mathrm{i}\xi_0/\sqrt{\hat{\Omega}}) - \mathrm{J}_{\nu+1}(-\mathrm{i}\xi_0/\sqrt{\hat{\Omega}})\mathrm{Y}_\nu(-\mathrm{i}\xi_0/\sqrt{\hat{\Omega}})} \tag{2.44b}$$

where $\xi_0 = \xi(t = 0)$ and $\hat{a}_{1,3} = a_{1,3}(t = 0)$. Owing to the symmetry, the solution to a_1 can be obtained from that of a_3 by switching a_3 with a_1.

To assist in understanding the basic characteristics of the solution for the growth of a_3 (and a_1), we consider the nearly perfect resonance case. With $\sigma/\omega_3 \ll 1$, the middle term on the left-hand side of (2.42) can be ignored. The general solution of the resulting equation is given as

$$a_3(\xi) = \mathbb{D}_1\mathrm{e}^{\xi/\sqrt{\hat{\Omega}}} + \mathbb{D}_2\mathrm{e}^{-\xi/\sqrt{\hat{\Omega}}} \tag{2.45}$$

where the constants $\mathbb{D}_1$ and $\mathbb{D}_2$ are determined from the initial condition. Depending on the signs of the interaction coefficients (B_{12} and B_{23}), the solution in (2.45) shows different characteristic behaviours. When B_{12} and B_{23} have the same sign (i.e. $\mathscr{B} > 0$), ξ is purely real and is proportional to $\exp(\hat{\Omega}^{1/2}t)$. As a result, $a_3 \sim \exp[\exp(\hat{\Omega}^{1/2}t)]$ which shows a bi-exponential growth with time. This suggests a highly efficient mechanism for transferring energy to linearly stable wave modes from a linearly unstable wave mode through triad resonant interaction. In the study of (wind) wave generation by a sheared current, Janssen (1987) predicted a similar energy transfer mechanism due to the nonlinear coupling between a linearly unstable mode and its

second harmonic. When B_{12} and B_{23} have different signs (i.e $\mathscr{B} < 0$), ξ is purely imaginary. In this case, $a_3 \sim \exp[\mathrm{i}\exp(\hat{\Omega}^{1/2}t)]$ which shows an oscillatory feature in time with a constant amplitude but an exponentially growing frequency. (Note that this result is consistent with the finding in the preceding section for the perfect resonance case with $\mathscr{B} < 0$.)

3. Numerical method

The theoretical analysis § 2 provides valuable insights into the dynamics of resonant triad wave interaction coupled with the Kelvin–Helmholtz instability effect for a two-fluid flow in a horizontal channel. To verify the theoretical prediction and deal with the practical situation involving multiple resonant interactions, we develop an effective numerical method that enables direct time simulation of the nonlinear initial boundary-value problem ((2.1)–(2.7)).

3.1. *Mathematical formulation of a high-order spectral method*

An efficient high-order pseudo-spectral (HOS) method, originally developed by Dommermuth & Yue (1987) for the study of nonlinear surface gravity waves, is modified to simulate the nonlinear interfacial evolution of stratified channel flows. The extension to nonlinear interactions of internal waves and surface waves over variable bottom topography was achieved by Alam, Liu & Yue (2009). This method solves the primitive equations of the problem by following the evolution of a large number of spectral interfacial wave modes and accounts for their interactions up to an arbitrarily high order of nonlinearity using a pseudo-spectral approach.

3.1.1. *Time evolution equations*

This process begins with the definition of the potentials at the interface within each fluid domain

$$\phi_u^I(x,t) = \phi_u(x,\eta(x,t),t) \tag{3.1a}$$

$$\phi_l^I(x,t) = \phi_l(x,\eta(x,t),t). \tag{3.1b}$$

Applying chain rule to (3.1) allows for the standard derivatives on the interface ($y=\eta$) to be written as

$$\frac{\partial\phi}{\partial t} = \frac{\partial\phi^I}{\partial t} - \frac{\partial\phi}{\partial y}\frac{\partial\eta}{\partial t}, \quad y=\eta \tag{3.2a}$$

$$\frac{\partial\phi}{\partial x} = \frac{\partial\phi^I}{\partial x} - \frac{\partial\phi}{\partial y}\frac{\partial\eta}{\partial x}, \quad y=\eta. \tag{3.2b}$$

With these new definitions of the potential derivatives, the boundary conditions maybe written as functions of the interface potentials. The kinematic boundary conditions (2.5) and (2.6) take the form

$$\frac{\partial\eta}{\partial t} = -\left[U_u + \frac{\partial\phi_u^I}{\partial x}\right]\frac{\partial\eta}{\partial x} + \left[1+\left(\frac{\partial\eta}{\partial x}\right)^2\right]\frac{\partial\phi_u}{\partial y}, \quad y=\eta \tag{3.3}$$

$$\frac{\partial\eta}{\partial t} = -\left[U_l + \frac{\partial\phi_l^I}{\partial x}\right]\frac{\partial\eta}{\partial x} + \left[1+\left(\frac{\partial\eta}{\partial x}\right)^2\right]\frac{\partial\phi_l}{\partial y}, \quad y=\eta \tag{3.4}$$

while the dynamic boundary condition, (2.7), is expressed as

$$\frac{\partial \Psi^I}{\partial t} = \frac{1}{2}\left[1+\left(\frac{\partial \eta}{\partial x}\right)^2\right]\left[\left(\frac{\partial \phi_l}{\partial y}\right)^2 - \mathscr{R}\left(\frac{\partial \phi_u}{\partial y}\right)^2\right] + \frac{1}{2}\left[\mathscr{R}\left(\frac{\partial \phi_u^I}{\partial x}\right)^2 - \left(\frac{\partial \phi_l^I}{\partial x}\right)^2\right] + \mathscr{R}U_u\frac{\partial \phi_u^I}{\partial x} - U_l\frac{\partial \phi_l^I}{\partial x} - (1-\mathscr{R})\eta + \frac{1}{\mathscr{W}}\frac{\eta_{xx}}{\left(1+\eta_x^2\right)^{3/2}}, \quad y=\eta \tag{3.5}$$

where $\Psi^I(x,t) \equiv \phi_l^I(x,t) - \mathscr{R}\phi_u^I(x,t)$. Together, (3.3) (or (3.4)) and (3.5) form a set of interfacial evolution equations that can be integrated in time to obtain the dynamic behaviour of the interface between the two fluids, provided that the interface velocities ($\partial\phi_u/\partial y$ and $\partial\phi_l/\partial y$ on $y=\eta$) and potentials (ϕ_u^I and ϕ_l^I) can be solved from the boundary-value problem.

3.1.2. *Perturbation expansions*

If it is assumed that ϕ_u, ϕ_l and η are $O(\epsilon) \ll 1$, where ϵ is a measure of the wave steepness, then these terms can be expanded in a perturbation series up to order M in terms of the small variable ϵ

$$\phi_{u/l}(x,y,t) = \sum_{m=1}^{M} \phi_{u/l}^{(m)}(x,y,t) \tag{3.6}$$

where $\phi_u^{(m)}$ and $\phi_l^{(m)}$ are $O(\epsilon^m)$. Since this is a free boundary problem, with ϕ_u, ϕ_l and η being unknown, we expand ϕ_u and ϕ_l on the interface ($y=\eta$) in Taylor series about the mean interface ($y=0$):

$$\phi_{u/l}(x,\eta,t) = \sum_{m=1}^{M}\phi_{u/l}^{(m)}(x,\eta,t) = \sum_{m=1}^{M}\sum_{k=0}^{M-m}\frac{\eta^k}{k!}\frac{\partial^k}{\partial y^k}\phi_{u/l}^{(m)}\bigg|_{y=0}. \tag{3.7}$$

It should be noted that the second summation is evaluated up to $M-m$ in order to maintain a consistent expansion up to $O(\epsilon^M)$.

Defining $\Psi(x,y,t) \equiv \phi_l(x,y,t) - \mathscr{R}\phi_u(x,y,t)$ and using (3.7) produces

$$\Psi^I(x,t) = \sum_{m=1}^{M}\Psi^{(m)}(x,\eta,t) = \sum_{m=1}^{M}\sum_{k=0}^{M-m}\frac{\eta^k}{k!}\frac{\partial^k}{\partial y^k}\Psi^{(m)}\bigg|_{y=0}. \tag{3.8}$$

If all terms of common order in (3.8) are collected, a set of Dirichlet boundary conditions for each $\Psi^{(m)}$ ($\equiv\phi_l^{(m)} - \mathscr{R}\phi_u^{(m)}$) on $y=0$ can be obtained as

$$\Psi^{(1)}(x,0,t) = \psi^I \tag{3.9}$$

$$\Psi^{(m)}(x,0,t) = -\sum_{k=1}^{m-1}\frac{\eta^k}{k!}\frac{\partial^k}{\partial y^k}\Psi^{(m-k)}\bigg|_{y=0}, \quad m=2,3,\ldots,M \tag{3.10}$$

with $\Psi^I(x,t)$ being obtained from the evolution equation (3.5) at any time t.

Taking the difference between (2.5) and (2.6) gives a new form of the kinematic interfacial boundary condition:

$$\Phi_y = \eta_x[\Phi_x + (U_u - U_l)], \quad y=\eta \tag{3.11}$$

where $\Phi \equiv \phi_u - \phi_l$. Applying the perturbation expansions for ϕ_u, ϕ_l and then expanding them in Taylor series about $y = 0$ yields

$$\Phi(x, \eta, t) = \sum_{m=1}^{M} \Phi^{(m)}(x, \eta, t) = \sum_{m=1}^{M} \sum_{k=0}^{M-m} \frac{\eta^k}{k!} \frac{\partial^k}{\partial y^k} \Phi^{(m)} \bigg|_{y=0}. \tag{3.12}$$

Substituting this expansion into (3.11), a set of Neumann boundary conditions can be obtained for each $\Phi_y^{(m)}$ on $y = 0$:

$$\Phi_y^{(1)}(x, 0, t) = \eta_x (U_u - U_l) \tag{3.13}$$

$$\Phi_y^{(m)}(x, 0, t) = \eta_x \sum_{k=1}^{m-1} \frac{\eta^{(k-1)}}{(k-1)!} \frac{\partial^{(k-1)}}{\partial y^{(k-1)}} \Phi_x^{(m-k)} \bigg|_{y=0} - \sum_{k=1}^{m-1} \frac{\eta^k}{k!} \frac{\partial^{(k+1)}}{\partial y^{(k+1)}} \Phi^{(m-k)} \bigg|_{y=0} \tag{3.14}$$

for $m = 2, 3, \ldots, M$.

With these expansions, the nonlinear boundary-value problem for ϕ_u, ϕ_l is decomposed into a sequence of linear boundary-value problems for the perturbed potentials $\phi_u^{(m)}$, $\phi_l^{(m)}$, $m = 1, 2, \ldots, M$, which can be solved sequentially starting from $m = 1$ up to an arbitrary order M.

3.1.3. *Solution of $\phi_u^{(m)}$ and $\phi_l^{(m)}$*

Assuming a periodic boundary condition in the x direction and choosing a normalization that makes the length of the computational domain $L = 2\pi$, the boundary-value solution at each order m, which satisfies both Laplace's equation and the zero-flux condition at the walls, can be written as a truncated Fourier series of the form

$$\phi_u^{(m)}(x, y, t) = \sum_{n=-N}^{N} A_n^{(m)}(t) \frac{\cosh k_n (y - h_u)}{\cosh k_n h_u} \mathrm{e}^{\mathrm{i}k_n x} \tag{3.15a}$$

$$\phi_l^{(m)}(x, y, t) = \sum_{n=-N}^{N} B_n^{(m)}(t) \frac{\cosh k_n (y + h_l)}{\cosh k_n h_l} \mathrm{e}^{\mathrm{i}k_n x} \tag{3.15b}$$

where the wavenumber of the nth Fourier mode $k_n = n$. From the Dirichlet boundary condition for $\Psi^{(m)}$ and the Neumann boundary condition for $\Phi^{(m)}$, the unknown Fourier modal amplitudes ($A_n^{(m)}$ and $B_n^{(m)}$) are determined to be

$$A_n^{(m)} = -\frac{\Phi_{yn}^{(m)} + \Psi_n^{(m)} k_n \tanh k_n h_l}{k_n (\tanh k_n h_u + \mathscr{R} \tanh k_n h_l)} \tag{3.16a}$$

$$B_n^{(m)} = \frac{\Psi_n^{(m)} k_n \tanh k_n h_u - \mathscr{R} \Phi_{yn}^{(m)}}{k_n (\tanh k_n h_u + \mathscr{R} \tanh k_n h_l)} \tag{3.16b}$$

for $n = -N, -N+1, \ldots, N$ but $n \neq 0$, where $\Psi_n^{(m)}$ and $\Phi_{yn}^{(m)}$ are the Fourier modal amplitudes of $\Psi^{(m)}(x, 0, t)$ and $\Phi_y^{(m)}(x, 0, t)$, respectively. For the mode of $n = 0$, the Dirichlet boundary condition requires that $B_0^{(m)} - \mathscr{R} A_0^{(m)} = \Psi_0^{(m)}$ while the Neumann boundary condition is automatically satisfied. For the complete solution of the problem, the specific values of $A_0^{(m)}$ and $B_0^{(m)}$ are not needed. For convenience in computation, we let $A_0^{(m)} = 0$ and $B_0^{(m)} = \Psi_0^{(m)}$.

After the boundary-value solutions of $\phi_u^{(m)}$ and $\phi_l^{(m)}$ are determined up to order M, the interface potentials ϕ_u^I and ϕ_l^I can be evaluated from (3.7). The interface

velocities, $\partial\phi_u/\partial y$ and $\partial\phi_l/\partial y$ on $y=\eta$, can be evaluated similarly by making Taylor series expansions about $y=0$ and then substituting the solutions of $\phi_u^{(m)}$ and $\phi_l^{(m)}$. The evolution equations (3.3) (or (3.4)) and (3.5) can be integrated in time (with properly defined initial conditions) by the use of any high-resolution integration method, such as the fourth-order Runge–Kutta scheme.

One notes that owing to the use of perturbation expansion (3.6) and spectral expansion (3.15), the boundary-value solution converges exponentially fast with increasing the order M and the number of spectral modes N for moderately steep interfaces. However, as the interface steepness increases, the convergence rate with M becomes slower. For steep waves, the present method is invalid because (3.6) will no longer converge with M. In this case, a fully nonlinear scheme needs to be applied.

This numerical method is designed for efficiently simulating the nonlinear evolution of an interface composed of broadbanded wave components. It is also equally capable of simulating the nonlinear evolution of a specific discrete set of wave modes. For these problems, a simple bandpass filter is applied at each time step to remove all non-relevant spectral components.

3.2. *Validation of the numerical method*

As a verification of the numerical method, a relatively simple case of a single triad resonance is considered in which the three interacting waves are all linearly stable. For this problem, a closed-form analytic solution is available. The evolution equations for the amplitudes of the interacting waves take the form (Campbell 2009):

$$\frac{\mathrm{d}a_1}{\mathrm{d}t} = \mathrm{i}B_{23}a_2a_3^*\mathrm{e}^{-\mathrm{i}\sigma t} \tag{3.17a}$$

$$\frac{\mathrm{d}a_2}{\mathrm{d}t} = \mathrm{i}b_{13}a_1a_3\mathrm{e}^{\mathrm{i}\sigma t} \tag{3.17b}$$

$$\frac{\mathrm{d}a_3}{\mathrm{d}t} = \mathrm{i}B_{12}a_1^*a_2\mathrm{e}^{-\mathrm{i}\sigma t} \tag{3.17c}$$

where the interaction coefficient b_{13} is

$$\begin{aligned} b_{13} = \frac{k_2}{4(\mathscr{R}\mathbb{D}_{u2}C_{u2}+\mathbb{D}_{l2}C_{l2})}&[\mathbb{D}_{l2}C_{l2}(\mathbb{D}_{l1}C_{l1}+\mathbb{D}_{l3}C_{l3})-\mathscr{R}\mathbb{D}_{u2}C_{u2}(\mathbb{D}_{u1}C_{u1}+\mathbb{D}_{u3}C_{u3})\\ &+\mathscr{R}(\mathbb{D}_{u1}^2+\mathbb{D}_{u3}^2)-(\mathbb{D}_{l1}^2+\mathbb{D}_{l3}^2)-\mathbb{D}_{l1}\mathbb{D}_{l3}(1-C_{l1}C_{l3})\\ &+\mathscr{R}\mathbb{D}_{u1}\mathbb{D}_{u3}(1-C_{u1}C_{u3})] \end{aligned} \tag{3.18}$$

and B_{12} and B_{23} are given by (2.26) in § 2.4.5. For perfect resonance ($\sigma=0$), (3.17) can be solved analytically with the solution given in terms of Jacobian elliptic functions (e.g. McGoldrick 1965). With initial amplitudes $a_1(0)=\hat{a}_1$, $a_2(0)=0$ and $a_3(0)=\hat{a}_3$, as an example, the solution takes the form

$$a_1 = \hat{a}_1\mathrm{dn}(\Xi\,|m) \tag{3.19a}$$

$$a_2 = \hat{a}_3\sqrt{\frac{b_{13}}{B_{12}}}\mathrm{sn}(\Xi\,|m) \tag{3.19b}$$

$$a_3 = \hat{a}_3\mathrm{cn}\,(\Xi\,|m) \tag{3.19c}$$

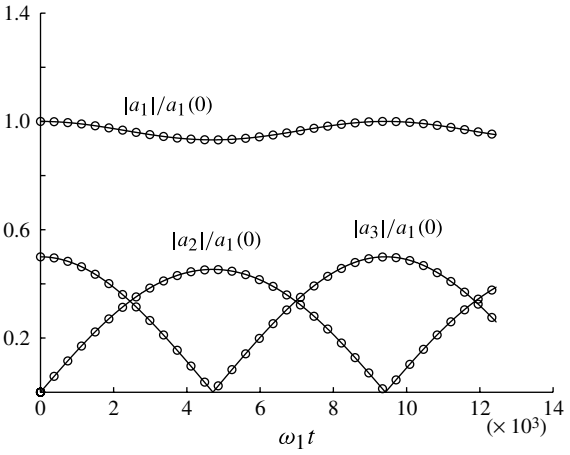

FIGURE 3. Time evolution of the amplitudes of primary waves in a resonant triad. The plotted curves represent the direct numerical simulation result with $M = 2$ (∘) and the theoretical prediction (——) by (3.19).

where dn, sn and cn are the Jacobian elliptic functions with arguments

$$\Xi = \hat{a}_1 \, (B_{13}B_{12})^{1/2} \, t, \quad m = \frac{B_{23}\hat{a}_3^2}{B_{12}\hat{a}_1^2} \leqslant 1. \tag{3.20}$$

Figure 3 compares the numerical simulation result (with order $M = 2$) with the analytic solution by (3.19) for the time variation of the amplitudes of interacting waves that form a resonant triad. As a numerical example, we use $\mathscr{R} = 1.23 \times 10^{-3}$, $\mathscr{W} \cong 845.5$, $H \equiv h_u + h_l \cong 1.25$, $\alpha \equiv h_u/H = 0.5$, $U_u \cong 7.94$, $U_l \cong 1.1$, $\hat{a}_1 \cong 6.28 \times 10^{-5}$, $\hat{a}_2 = 0$, $\hat{a}_3 = \hat{a}_1/2$ and $L = 2\pi$. The interacting waves have wavenumbers $k_1 = 11$, $k_2 = 46$ and $k_3 = 35$. (With normalization length $\mathscr{L} \cong 0.08$ m and time $\mathscr{T} \cong 0.09$ s, as an example, these dimensionless parameters correspond to an air–water flow in a horizontal channel in a laboratory scale with $H = 0.1$ m, $L = 0.5$ m, $U_u \cong 7.0$ m s^{-1}, $U_l = 1.0$ m s^{-1}, $\gamma = 0.0734$ N m^{-1} and $\hat{a}_1 = 10^{-6}$ m). Excellent agreements between the numerical simulation result (of the leading order) and the analytic solution are shown and thus validate the numerical method. The numerical simulation result with $M = 3$ is graphically indistinguishable from that with $M = 2$. Thus, it is not shown in the figure. Note that the fluid properties used in this example correspond to those of air and water. They are chosen because these two fluids are commonly used in laboratory experiments; however, the theory and direct computation are applicable to general two-phase flows.

4. Results

In this section, we describe the characteristic features of triad resonant interfacial wave interactions, which are influenced by the Kelvin–Helmholtz instability, in a two-fluid channel flow. To assist in understanding the solution, the nonlinear self-interaction effects on the Kelvin–Helmholtz instability are first investigated. Both theoretical solutions, based on the analysis in § 2 and direct numerical simulation results using the method outlined in § 3 are presented and discussed.

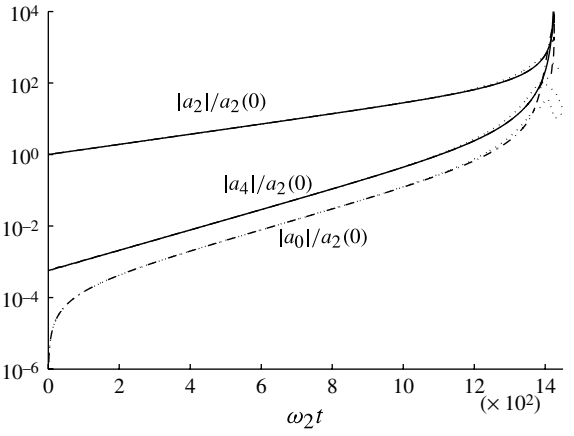

FIGURE 4. Time evolution of the amplitudes of the primary wave (a_2), second harmonic (a_4) and zeroth harmonic (a_0). The plotted curves represent the theoretical solution (——) and numerical simulations with order $M = 2$ (· · ·) and $M = 3$ (— · —).

For numerical illustration, we use the same flow conditions as described in § 3.2 with the exception that $U_u = U_l + U_c(1 + \Delta)$, where U_c is given by (2.11) and Δ is chosen to be 10^{-4}. The initial condition for the primary waves is chosen to be $a_2(0) = 1.25 \times 10^{-5}$, $a_1(0) = 1/2a_2(0)$, $a_3(0) = 0$ and $\phi_{u0}(0) = \phi_{l0}(0) = 0$. The initial amplitudes of the primary waves are intentionally chosen to be small so that the associated velocity potentials at $t = 0$ are properly given by the linear solution. This also allows for a longer period of nonlinear growth before the waves become too steep for the perturbation-based analysis and simulation. The initial condition for the second harmonic is given in terms of the primary wave by (2.21). This set of initial conditions are sufficient for direct numerical simulation since the evolution equations ((3.3) or (3.4)) and (3.5) only contain the first-order time derivatives. The theoretical model also requires $\dot{a}_2(0)$ and $\dot{\phi}_{l0}(0) - \mathscr{R}\dot{\phi}_{u0}(0)$ since the second-order time derivative is present in (2.37*a*). We use $\dot{a}_2(0) = a_2(0)\sqrt{\Omega}$ based on the linear growth rate of k_2 wave, and let $\dot{\phi}_{l0}(0) - \mathscr{R}\dot{\phi}_{u0}(0)$ be equal to the initial value obtained in the numerical simulation (in order for direct comparison between the theoretical solution and the numerical simulation to be consistent).

This set of flow properties and initial conditions are used for the results presented in this section unless stated otherwise.

4.1. *Self-interactions*

By removing the term associated with the interaction of k_1 and k_3 waves in (2.37*a*), we obtain an evolution equation for the amplitude a_2 of the slightly unstable k_2 wave including the effect of third-order self-interactions. The equation clearly indicates that depending on the sign of the parameter $\hat{\mathscr{N}}$, the inclusion of the third-order self-interaction effect can accelerate or stabilize the growth of k_2 wave as its amplitude becomes larger due to the linear instability effect.

Figure 4 shows the time evolution of the amplitude a_2 of an unstable wave with wavenumber $k_2 = 25$ for which $\hat{\mathscr{N}} \simeq 4 \times 10^4$. The results for the second and zeroth harmonics are also shown. The evolution equation (cf. (2.37*a*)) clearly shows that initially the growth of a_2 is dominated by the linear instability. This growth of a_2

continues according to linear theory until the third-order self-interaction term becomes significant. Since $\hat{\mathscr{N}} > 0$, the third-order self-interaction increases the growth rate of a_2 above that of the linear solution. This nonlinear effect is stronger as a_2 becomes larger in the evolution. As time increases, the growth rate continues to increase until the amplitude of a_2 rapidly becomes unbounded, as shown in figure 4. The second harmonic is a locked wave that is stable in this case. Thus, it grows at twice the rate of a_2. For the zeroth harmonic, the leading-order theoretical solution is a near-zero constant. The next order solution is not pursued in this study.

The direct numerical simulation results ($M = 2, 3$) compare excellently with the theoretical prediction for both the primary wave and its second harmonic until the very late stage of evolution when the solution quickly blows up. The numerical solution is convergent with order M since the solution of $M = 2$ agrees well with that of $M = 3$ except at the late stage where the third-order effects become apparent. The numerical simulation also provides a prediction for the zeroth harmonic that is generally about one order smaller than the second harmonic except at the late stage of evolution when the solution quickly becomes singular. One notes that as the wave amplitude a_2 becomes considerably large at late stage of evolution, higher-order effects are important, which are not considered in the theoretical analysis. While the simulation can include such higher-order effects, it will eventually fail to converge with M as wave steepness continues to increase since the numerical simulation is based on a perturbation approach.

A numerical search over a wide range of flow parameters suggests that the case of $\hat{\mathscr{N}} < 0$ occurs only when the second harmonic of the k_2 wave is also linearly unstable. The theoretical analysis in § 2 does not apply to this case since the analysis assumes a linearly stable second harmonic. In this case, strong interactions between the primary wave and its second harmonic, called an overtone resonance, can occur. This itself is an interesting topic in nonlinear interfacial wave dynamics and is pursued in a separate study.

4.2. *Triad resonant interactions*

We now turn to the study of triad resonant interaction that involves one unstable and two stable interacting wave components. The discussion in § 2.5 indicates that different characteristic solutions exist depending on the sign of the parameter $\mathscr{B} \equiv B_{12}/B_{23}$. Both cases are considered here.

4.2.1. $\mathscr{B} < 0$

For this example the triad resonance consists of the interacting waves with wavenumbers $k_1 = 24$, $k_2 = 25$ and $k_3 = 1$ which produces $\hat{\mathscr{N}} \simeq 4 \times 10^4$ and $\mathscr{B} \simeq -0.017$. The k_2 wave is slightly unstable. The resulting evolution of the amplitudes of these waves, as well as the second harmonic of k_2 wave and the zeroth harmonic, is shown in figure 5.

The analytic solution demonstrates that the amplitudes of the k_2 wave, its second harmonic and the zeroth harmonic behave similarly to the case without the involvement of the triad resonance interaction, discussed in § 4.1. The growth of a_2 is dominated by the linear instability while the second harmonic, which is locked to a_2, grows with twice the linear growth rate of a_2. As a_2 becomes large, the positive nonlinear self-interaction term causes the growth rate to continuously increase until the solution becomes singular. This singularity causes the second harmonic to become singular as well. The theoretical solution predicts that the zeroth harmonic maintains a near-zero constant amplitude during the entire evolution. In this case, the amplitude

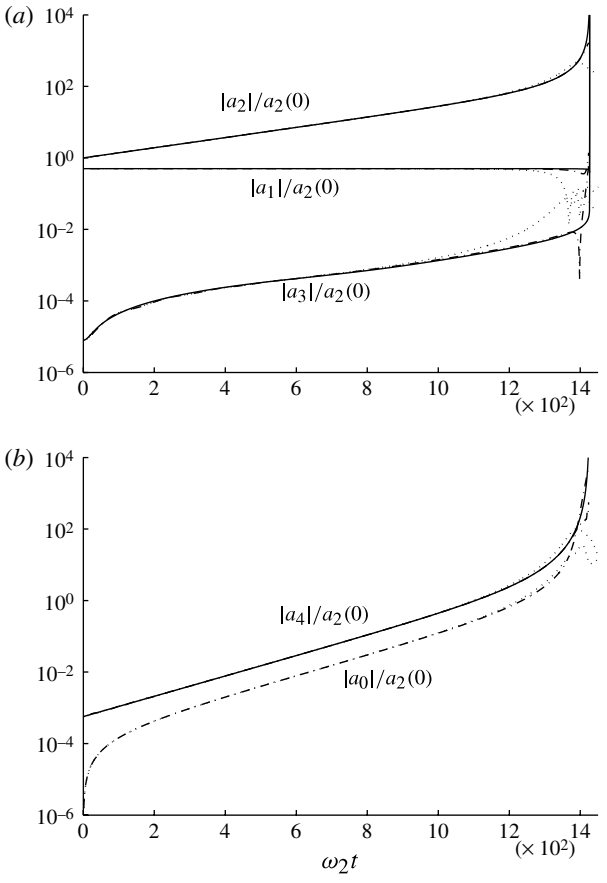

FIGURE 5. Time evolution of the amplitudes of (*a*) primary waves (a_2, a_1 and a_3) and (*b*) second harmonic of k_2 wave (a_4) and zeroth harmonic (a_0). The plotted curves represent the theoretical solution (——) and numerical simulations with order $M = 2$ (· · ·) and $M = 3$ (— · —).

of the k_1 wave (a_{k_1}) remains almost unchanged. For the k_3 wave, a_3 grows rapidly from its much smaller initial value by taking energy from the other two primary waves through the triad resonance. During the later stage, as a_3 becomes about two orders of magnitude smaller than a_1, the growth rate of a_3 significantly decreases. Despite the continuous growth, a_3 remains about two orders of magnitude smaller than a_1 until the solution of the system becomes singular. During the entire evolution, the sum of energy of the k_1 and k_3 wave remains unchanged as predicted by the analysis in § 2.5.1 (even though the k_2 wave grows significantly).

The direct simulation results show good agreements with the analytic solution except at the very late stage of evolution when the higher-order effects become important and the unstable k_2 wave is developed significantly. At this stage of evolution, the numerical solution clearly indicates that the growth of a_3 is obtained due to the decrease of a_1 as predicted by the theory with $\mathscr{B} < 0$ in § 2.5.1.

One notes that in this case, the growth of the k_3 wave is resulted with the energy transfer from the stable k_1 wave, but not from the unstable k_2 wave. Thus, this type

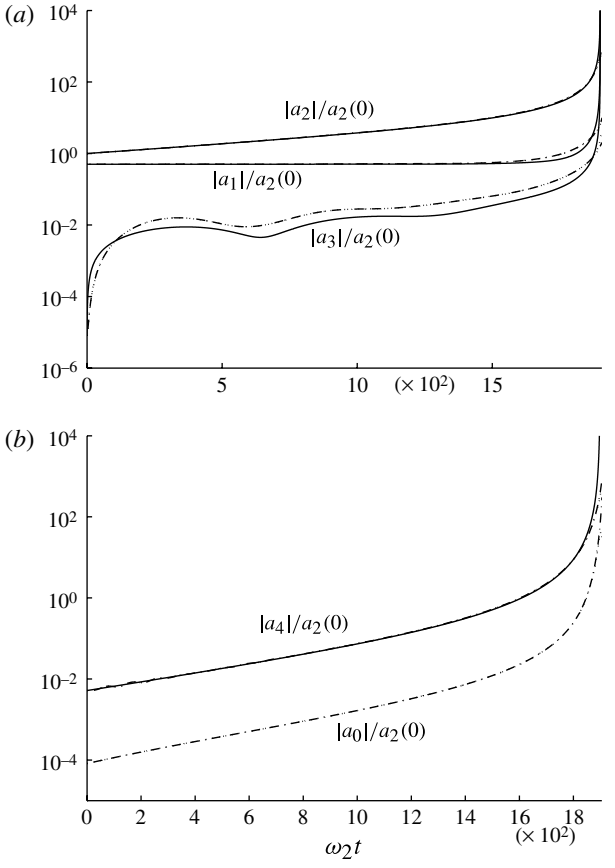

FIGURE 6. Time evolution of the amplitudes of (*a*) primary waves (a_2, a_1 and a_3) and (*b*) second harmonic of k_2 wave (a_4) and zeroth harmonic (a_0). The plotted curves represent the theoretical solution (——) and numerical simulations with order $M = 2$ (· · ·) and $M = 3$ (— · —).

of triad resonance (with $\mathscr{B} < 0$) does not provide a significant energy build up for long waves.

4.2.2. $\mathscr{B} > 0$

The analysis in § 2.5.1 indicates that for $\mathscr{B} > 0$ it is possible for a_1 and a_3 to grow without bound. Figure 6 shows such a sample solution. This solution is obtained with the same air–water flow as before, but with $\alpha = 0.05$, $k_1 = 11$, $k_2 = 12$, and $k_3 = 1$, which produces $\hat{\mathscr{N}} \simeq 1.414 \times 10^5$ and $\mathscr{B} \simeq 0.053$. At the initial stage of evolution, as the analysis in § 2.5.2 shows, a_2 is dominated by the linear instability effect, and the initial growth rate of a_3 is bi-exponential as shown in figure 7. During the later stage of the evolution, the growth of a_2 is accelerated by the third-order self-interactions. As a result, both a_1 and a_3 obtain a growth rate even faster than bi-exponential as shown in figure 8. The interacting wave system then quickly blows up. The prediction by direct numerical simulations compares very well with the theoretical solution until the late stage of evolution when the interacting waves grow rapidly and become singular.

For the second harmonic of the k_2 wave, the analytical solution also agrees well with the numerical solution. Both solutions predict that the second harmonic eventually

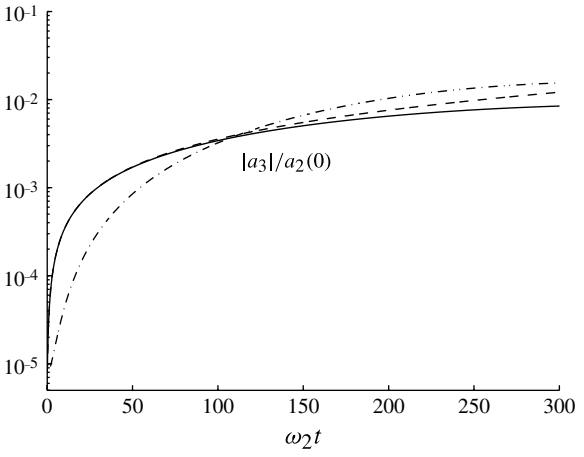

FIGURE 7. Close-up of initial growth of the k_3 wave mode in figure 6(a). The plotted curves represent the theoretical solution (——) and the approximate solution (2.45) (- - -).

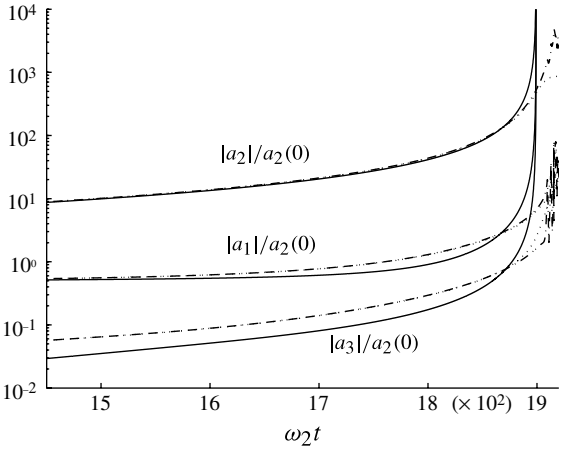

FIGURE 8. Close-up of the later bi-exponential growth of the k_3 wave mode in figure 6(a). The plotted curves represent the theoretical solution (——) and numerical simulations with order $M = 2$ ($\cdot\ \cdot\ \cdot$) and $M = 3$ (— $\cdot$ —).

becomes unbounded like the primary waves. For the zeroth harmonic, the analytic solution predicts a near-zero constant amplitude while the numerical solution shows that the amplitude of the zeroth harmonic increases together with the other wave modes and also becomes unbounded eventually.

We remark that in this case, stable waves are developed significantly by the energy transfer from the unstable wave through triad resonant wave interactions. This type of triad resonance (with $\mathscr{B} > 0$) provides an effective mechanism for transferring energy from unstable short waves to stable long waves, leading to a fast development of large-amplitude long waves in a two-fluid channel flow.

4.3. *Multiple resonant interactions*

Realistic two-fluid flow problems involve a broadbanded spectrum of interfacial waves that can form multiple coupled triad resonant (and near-resonant) interactions. Moreover, as the interface steepens, higher-order resonant interactions may also play a role. Large-amplitude long waves can be developed due to the combined effects of the linear instability and multiple resonant interactions. The extension of the theoretical analysis in § 2 to include multiple coupled resonant interactions is in principle possible, but not straightforward. The direct numerical simulation developed in § 3 is more appropriate for these practical cases.

As a numerical example, we consider the growth and time evolution of a large-amplitude long wave that is developed from a smooth interface in a two-phase channel flow. The spectrum shall be broadbanded and contain multiple resonant triads. This problem will approximate the spacial evolution of the first slug developed near the inlet of the two-phase channel flow. While there is a rich collection of laboratory experiments in the literature, the vast majority of these tests are carried out using cylindrical pipe geometries (e.g. Fan *et al.* 1993). Ideally, comparisons between numerical simulations and measurements should be made with identical geometry. However, to obtain an initial estimate, the numerical simulations presented here are performed using the same flow properties as those in pipe flow experiments.

We choose to compare the direct simulations against the results of Ujang (2003) and Ujang *et al.* (2006) who carried out experiments of air–water flows through a horizontal 78 mm pipe with different gas/liquid velocities and liquid holdups. We specifically focus on the case of figure 5(*c*) of Ujang *et al.* (2006) or figure 5.3(*a*) of Ujang (2003) for which the superficial gas and liquid velocities $U_{SG} \equiv U_u A_u/A_{pipe} = 4.64$ m s^{-1} and $U_{SL} \equiv U_l A_l/A_{pipe} = 0.61$ m s^{-1} with A_{pipe}, A_u and A_l being the cross-sectional area of the pipe and the areas of the pipe occupied by the upper and lower fluids, respectively. The gas fraction for the pipe is $\backsimeq 0.4$ and the surface tension coefficient is 0.037 N m^{-1}. In the simulation, the channel depth is set to be equal to the pipe diameter ($H = 78$ mm) and the void fraction is fixed as $\alpha = 0.4$. The uniform gas and liquid velocities are $U_u = U_{SG}A_{pipe}/A_G = 12.53$ m s^{-1} and $U_l = U_{SL}A_{pipe}/A_L = 0.97$ m s^{-1}.

In the numerical computation, we use $\mathscr{L} = 0.318$ m and $\mathscr{T} = 0.180$ s for length and time normalization. The length of the (periodic) computational domain corresponds to a laboratory channel length of 2.0 m. The density ratio is $\mathscr{R} = 1.18 \times 10^{-3}$ and the Weber number is $\mathscr{W} = 2.67 \times 10^4$. The simulations are performed with $N = 32$ and different orders of nonlinearity ($M = 1$, 2 and 3). The initial disturbance on the interface is given by the white noise with a near machine-zero amplitude of 10^{-15}. We note that in reality, the growth of very short waves are limited by viscous damping and small-scale wave breaking which are not considered in the simulation based on the potential flow formulation. Since our purpose is to demonstrate the growth of long waves through multiple/coupled resonant interactions with short waves, a spectral filtering is applied in the nonlinear simulations (with $M = 2$ and 3) to limit the maximum steepness of each of the unstable short-wave component (with $k > 17$) at $0.1\,\mathrm{sech}(0.05k)$. This approach was developed by Longuet-Higgins & Cokelet (1976) and Dommermuth & Yue (1987) in the simulation of nonlinear breaking waves in the ocean.

Figure 9(*a,c,e*) show the amplitude spectra of the interface at $t = 0.844$, 1.410 and 1.834 s during the evolution of the two-phase channel flow. The simulation results obtained with $M = 1$, 2 and 3 are compared. The corresponding interfacial shape is shown in figure 9(*b,d,f*). The results in these figures indicate that the same energy

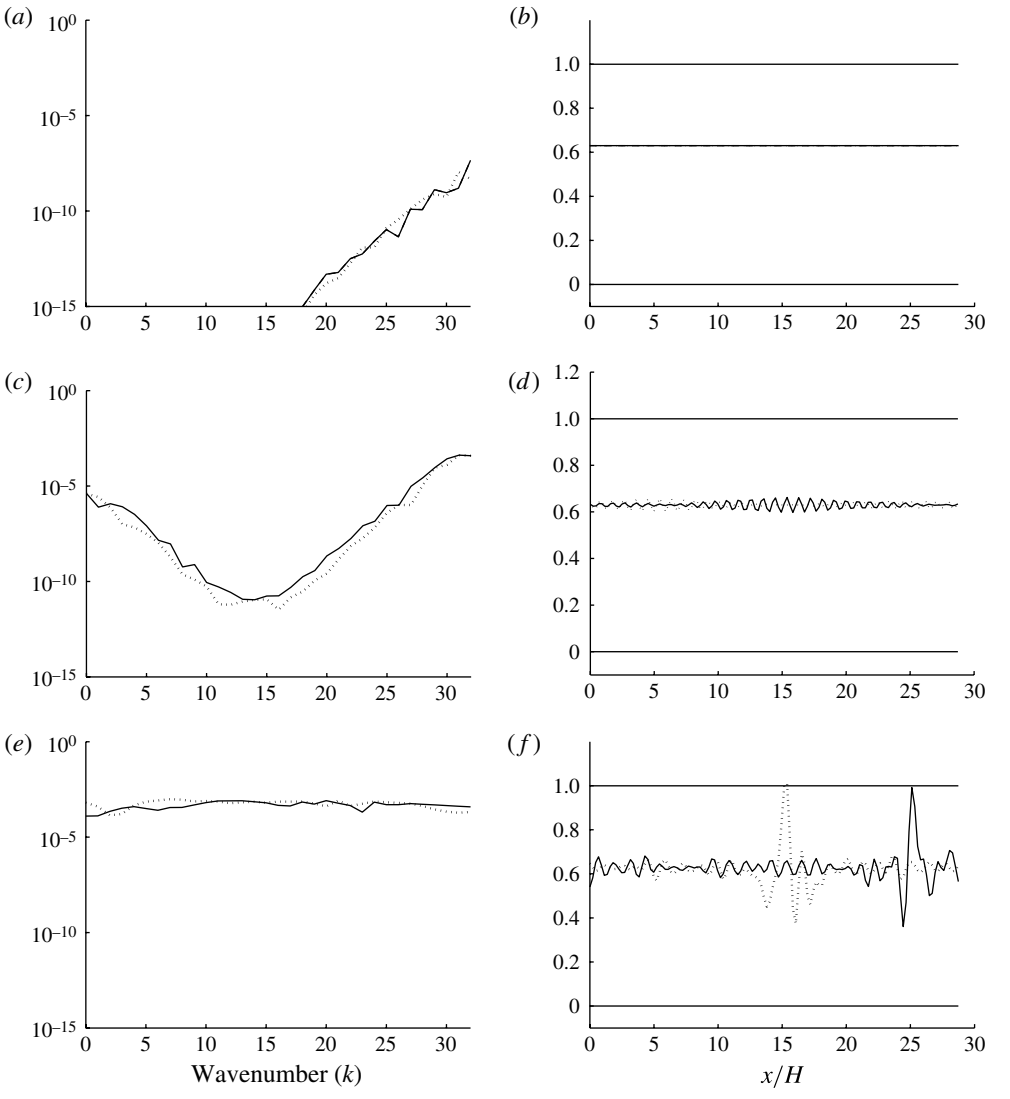

FIGURE 9. The nonlinear simulation of the time evolution of broadbanded interfacial waves in a air–water channel flow. (*a,c,e*) The distribution of spectral amplitude (normalized by $\mathscr{L}$) of interfacial wave components with $M = 1$ (- - -), $M = 2$ (——), and $M = 3$ ($\cdot\ \cdot\ \cdot$). (*b,d,f*) The corresponding interface shape, $(\eta + h_l)/H$.

transfer mechanism described in § 4.2 is observed in the presence of multiple resonant and near-resonant interactions. The linearly unstable spectral modes (with $k > 17$) initially grow due to the Kelvin–Helmholtz mechanism as shown in figure 9(*a,b*). As their amplitudes increase and the nonlinearity becomes stronger, some of the energy supplied by the linear instability is transferred to the long-wave components through multiple resonant interactions, as evidenced by the presence of two apparent peaks in the spectrum shown in figure 9(*c*). As this nonlinear process continues, the wave spectrum of the interface becomes broadbanded, resulting in the formation of a large-amplitude wave whose crest eventually touches the top boundary of the channel, as depicted in figure 9(*e,f*).

For this case, the interface bridges the channel diameter after $t \sim 1.83$ s of evolution. The width of the large wave disturbance is $\sim 1.8H$. By multiplying this time by the group velocity of the wave with wavelength of $\sim 1.8H$, where $C_g \cong 1.0$ m s^{-1}, we obtain the slug-initiation distance of approximately 1.85 m from the inlet (Gaster 1962). The difference in the nonlinear solutions with $M = 2$ and 3 are small until times just prior to the instant when the long-wave crest touches the top boundary. The simulation with $M = 1$ bridges the channel at much earlier time than the $M = 2$ and 3 cases, thus it is not shown in figure 9(*c*,*f*). This result compares qualitatively well with the experimental observation of Ujang (2003) who reported that first slugging occurred in the region of 1.46–2.86 m from the inlet. Even though this comparison is only a first-order estimate, this method appears to consistently reproduce results which have comparable length and times scales to the cases in figure 5 of Ujang (2003).

5. Conclusions

This paper has considered, both theoretically and computationally, the triad resonant interactions of interfacial waves, which are influenced by the Kelvin–Helmholtz interfacial instability, in an inviscid two-fluid incompressible flow through a horizontal channel. The focus is on the mechanism of energy transfer from unstable short waves to stable long waves through nonlinear resonant wave interactions. Based on a multiple-scale analysis, in the context of a potential flow formulation, nonlinear interaction equations are derived which govern the amplitude evolution of the interacting waves in a resonant triad, including the effects of interfacial instability. An effective numerical method for direct simulations of nonlinear interfacial wave interactions is also developed based on a high-order pseudo-spectral approach. It is used for verification of the theoretical analysis and the examination of practical applications involving multiple resonances with a broadbanded spectrum of waves. Cross-validations between the theoretical solutions and direct numerical simulations are obtained for various characteristic flows considered.

It is found that depending on the flow conditions, there exists an extremely efficient energy transfer from the base flow to the stable long wave due to the coupled effects of nonlinear wave resonance and interfacial instability. The growth rate of the long wave can reach up to bi-exponential (or faster). Moreover, in this case, the (linearly) unstable wave can grow unboundedly even when the nonlinear self-interaction effects are accounted for, as do the stable waves in the resonant triad.

This work shows that the nonlinear coupling of an interfacial instability and nonlinear resonant wave interactions can cause a rapid development of long waves (which are themselves linearly stable). Such a behaviour of long-wave growth bears similarities to that of slug formation in stratified channel/pipe flows, as observed in experiments. This suggests that the nonlinear mechanism found in this study may play an important role in slug formation and may improve slug-transition criteria. As a demonstration, we performed direct numerical simulations of nonlinear two-phase channel flow evolution involving multiple resonant and near-resonant wave interactions. The predicted slug-initiation length compares qualitatively well with the laboratory measurement. The application of the present work to the general multi-phase flow problem for development of improved slug flow transition criteria, prediction of slug frequency/length and direct comparisons with experimental measurements is the focus of ongoing research.

Acknowledgements

This work was financially supported by Chevron Corporation. Their sponsorship is greatly appreciated. We would also like to thank Dr R. Roberts and Dr K. Hendrickson for their thoughtful discussions and feedback on the subject.

Appendix. Perturbation equations

Based on the definitions of the two time scales, the differential time operator in (2.5)–(2.7), $\partial/\partial t$, is replaced by $\partial/\partial t + \Delta^{1/2}\partial/\partial\tau$, which leads to

$$\nabla^2\phi_u = 0 \quad \text{(A 1}a\text{)}$$

$$\nabla^2\phi_l = 0 \quad \text{(A 1}b\text{)}$$

$$\phi_{u,y} = 0 \quad \text{(A 1}c\text{)}$$

$$\phi_{l,y} = 0 \quad \text{(A 1}d\text{)}$$

$$\eta_{,t} + \Delta^{1/2}\eta_{,\tau} + [U_l + U_c(1+\Delta) + \phi_{u,x}]\eta_{,x} - \phi_{u,y} = 0 \quad \text{(A 1}e\text{)}$$

$$\eta_{,t} + \Delta^{1/2}\eta_{,\tau} + (U_l + \phi_{l,x})\eta_{,x} - \phi_{l,y} = 0 \quad \text{(A 1}f\text{)}$$

$$\mathscr{R}\left\{\phi_{u,t} + \Delta^{1/2}\phi_{u,\tau} + \frac{1}{2}\phi_{u,x}^2 + [U_l + U_c(1+\Delta)]\phi_{u,x} + \frac{1}{2}\phi_{u,y}^2 + \eta\right\}$$
$$- \left(\phi_{l,t} + \Delta^{1/2}\phi_{l,\tau} + \frac{1}{2}\phi_{u,x}^2 + U_l\phi_{l,x} + \frac{1}{2}\phi_{l,y}^2 + \eta\right) + \frac{\eta_{,xx}(1+\eta_x^2)^{-3/2}}{\mathscr{W}} = 0. \quad \text{(A 1}g\text{)}$$

Expanding (A 1e), (A 1f) and (A 1g) in Taylor series about the undisturbed interface position and applying (2.14) gives rise to a sequence of governing equations for $\phi_u^{(m)}$, $\phi_l^{(m)}$, and $\eta^{(m)}$, $m = 1, \ldots, 5$:

$$\nabla^2\phi_u^{(m)} = 0 \quad \text{(A 2}a\text{)}$$

$$\nabla^2\phi_l^{(m)} = 0 \quad \text{(A 2}b\text{)}$$

$$\phi_{u,y}^{(m)} = 0 \quad \text{(A 2}c\text{)}$$

$$\phi_{l,y}^{(m)} = 0 \quad \text{(A 2}d\text{)}$$

$$\eta_{,t}^{(m)} + (U_l + U_c)\eta_{,x}^{(m)} - \phi_{u,y}^{(m)} = f_1^{(m)} \quad \text{(A 2}e\text{)}$$

$$\eta_{,t}^{(m)} + U_l\eta_{,x}^{(m)} - \phi_{l,y}^{(m)} = f_2^{(m)} \quad \text{(A 2}f\text{)}$$

$$\mathscr{R}[\phi_{u,t}^{(m)} + (U_l + U_c)\phi_{u,x}^{(m)} + \eta^{(m)}] - [\phi_{l,t}^{(m)} + U_l\phi_{l,x}^{(m)} + \eta^{(m)}] + \frac{\eta_{,xx}^{(m)}}{\mathscr{W}} = f_3^{(m)}. \quad \text{(A 2}g\text{)}$$

where $f_j^{(1)} = 0$ and $f_j^{(2)} = 0$, $j = 1, 2, 3$ and $f_j^{(m)}$ for $m = 3$, 4 and 5 are functions of the lower-order solutions.

The $O(\Delta)$ problem:

$$f_1^{(3)} = -\eta_{,\tau}^{(1)} - \phi_{u,x}^{(1)}\eta_{,x}^{(1)} + \eta^{(1)}\phi_{u,yy}^{(1)} \quad \text{(A 3}a\text{)}$$

$$f_2^{(3)} = -\eta_{,\tau}^{(1)} - \phi_{l,x}^{(1)}\eta_{,x}^{(1)} + \eta^{(1)}\phi_{l,yy}^{(1)} \quad \text{(A 3}b\text{)}$$

$$f_3^{(3)} = [\eta^{(1)}\phi_{l,ty}^{(1)} + \phi_{l,\tau}^{(1)} + \tfrac{1}{2}(\phi_{l,x}^{(1)})^2 + U_l\eta^{(1)}\phi_{l,xy}^{(1)} + \tfrac{1}{2}(\phi_{l,y}^{(1)})^2]$$
$$- \mathscr{R}[\eta^{(1)}\phi_{u,ty}^{(1)} + \phi_{u,\tau}^{(1)} + \tfrac{1}{2}(\phi_{u,x}^{(1)})^2 + (U_l + U_c)\eta^{(1)}\phi_{u,xy}^{(1)} + \tfrac{1}{2}(\phi_{u,y}^{(1)})^2]. \quad \text{(A 3}c\text{)}$$

The $O(\Delta^{5/4})$ problem:

$$f_1^{(4)} = -\eta_{,\tau}^{(2)} - \eta_{,x}^{(1)}\phi_{u,x}^{(2)} - \eta_{,x}^{(2)}\phi_{u,x}^{(1)} + \eta^{(1)}\phi_{u,yy}^{(2)} + \eta^{(2)}\phi_{u,yy}^{(1)} \tag{A 4a}$$

$$f_2^{(4)} = -\eta_{,\tau}^{(2)} - \eta_{,x}^{(1)}\phi_{l,x}^{(2)} - \eta_{,x}^{(2)}\phi_{l,x}^{(1)} + \eta^{(1)}\phi_{l,yy}^{(2)} + \eta^{(2)}\phi_{l,yy}^{(1)} \tag{A 4b}$$

$$\begin{aligned} f_3^{(4)} = {} & [\eta^{(1)}\phi_{l,ty}^{(2)} + \eta^{(2)}\phi_{l,ty}^{(1)} + \phi_{l,\tau}^{(2)} + \phi_{l,x}^{(1)}\phi_{l,x}^{(2)} + U_l(\eta^{(1)}\phi_{l,xy}^{(2)} + \eta^{(2)}\phi_{l,xy}^{(1)}) \\ & + \phi_{l,y}^{(1)}\phi_{l,y}^{(2)}] - \mathscr{R}[\eta^{(1)}\phi_{u,ty}^{(2)} + \eta^{(2)}\phi_{u,ty}^{(1)} + \phi_{u,\tau}^{(2)} + \phi_{u,x}^{(1)}\phi_{u,x}^{(2)} \\ & + (U_l + U_c)(\eta^{(1)}\phi_{u,xy}^{(2)} + \eta^{(2)}\phi_{u,xy}^{(1)}) + \phi_{u,y}^{(1)}\phi_{u,y}^{(2)}]. \end{aligned} \tag{A 4c}$$

The $O(\Delta^{3/2})$ problem:

$$\begin{aligned} f_1^{(5)} = {} & -\eta_{,\tau}^{(3)} - U_c\eta_{,x}^{(1)} - \eta_{,x}^{(1)}\phi_{u,x}^{(3)} - \eta_{,x}^{(3)}\phi_{u,x}^{(1)} - \eta^{(1)}\phi_{u,xy}^{(1)}\eta_{,x}^{(1)} - \eta_{,x}^{(2)}\phi_{u,x}^{(2)} \\ & + \eta^{(1)}\phi_{u,yy}^{(3)} + \eta^{(3)}\phi_{u,yy}^{(1)} + \eta^{(2)}\phi_{u,yy}^{(2)} + \frac{1}{2}(\eta^{(1)})^2\phi_{u,yyy}^{(1)} \end{aligned} \tag{A 5a}$$

$$\begin{aligned} f_2^{(5)} = {} & -\eta_{,\tau}^{(3)} - \eta_{,x}^{(1)}\phi_{l,x}^{(3)} - \eta_{,x}^{(3)}\phi_{l,x}^{(1)} - \eta^{(1)}\phi_{l,xy}^{(1)}\eta_{,x}^{(1)} - \eta_{,x}^{(2)}\phi_{l,x}^{(2)} + \eta^{(1)}\phi_{l,yy}^{(3)} \\ & + \eta^{(3)}\phi_{l,yy}^{(1)} + \eta^{(2)}\phi_{l,yy}^{(2)} + \frac{1}{2}(\eta^{(1)})^2\phi_{l,yyy}^{(1)} \end{aligned} \tag{A 5b}$$

$$\begin{aligned} f_3^{(5)} = {} & \Bigg[\eta^{(1)}\phi_{l,ty}^{(3)} + \eta^{(3)}\phi_{l,ty}^{(1)} + \eta^{(2)}\phi_{l,ty}^{(2)} + \frac{1}{2}(\eta^{(1)})^2\phi_{l,tyy}^{(1)} + \phi_{l,\tau}^{(3)} + \phi_{l,x}^{(1)}\phi_{l,x}^{(3)} \\ & + \eta^{(1)}\phi_{l,x}^{(1)}\phi_{l,xy}^{(1)} + \frac{1}{2}(\phi_{l,x}^{(2)})^2 + U_l\left(\eta^{(1)}\phi_{l,xy}^{(3)} + \eta^{(2)}\phi_{l,xy}^{(2)} + \eta^{(3)}\phi_{l,xy}^{(1)} + \frac{1}{2}(\eta^{(1)})^2\phi_{l,xyy}^{(1)}\right) \\ & + \phi_{l,y}^{(1)}\phi_{l,y}^{(3)} + \eta^{(1)}\phi_{l,y}^{(1)}\phi_{l,yy}^{(1)} + \frac{1}{2}(\phi_{l,y}^{(2)})^2\Bigg] - \mathscr{R}\left[\eta^{(1)}\phi_{u,ty}^{(3)} + \eta^{(3)}\phi_{u,ty}^{(1)} + \eta^{(2)}\phi_{u,ty}^{(2)}\right. \\ & + \frac{1}{2}(\eta^{(1)})^2\phi_{u,tyy}^{(1)} + \phi_{u,\tau}^{(3)} + \phi_{u,x}^{(1)}\phi_{u,x}^{(3)} + \eta^{(1)}\phi_{u,x}^{(1)}\phi_{u,xy}^{(1)} + \frac{1}{2}(\phi_{u,x}^{(2)})^2 \\ & + U_c\phi_{u,x}^{(1)}(U_l + U_c)(\eta^{(1)}\phi_{u,xy}^{(3)} + \eta^{(2)}\phi_{u,xy}^{(2)} + \eta^{(3)}\phi_{u,xy}^{(1)} + \frac{1}{2}(\eta^{(1)})^2\phi_{u,xyy}^{(1)}) + \phi_{u,y}^{(1)}\phi_{u,y}^{(3)} \\ & \left. + \eta^{(1)}\phi_{u,y}^{(1)}\phi_{u,yy}^{(1)} + \frac{1}{2}(\phi_{u,y}^{(2)})^2\right] + \frac{3}{2}\frac{(\eta_{,x}^{(1)})^2\eta_{,xx}^{(1)}}{\mathscr{W}}. \end{aligned} \tag{A 5c}$$

REFERENCES

ALAM, M.-R., LIU, Y. & YUE, D. K. P. 2009 Bragg resonance of waves in a two-layer fluid propagating over bottom ripples. Part II. Numerical simulation. *J. Fluid Mech.* **624**, 225–253.

BARNEA, D. & TAITEL, Y. 1993 Kelvin–Helmholtz stability-criteria for stratified flow—viscous versus non-viscous (inviscid) approaches. *Intl J. Multiphase Flow* **19** (4), 639–649.

BENNEY, D. J. 1962 Non-linear gravity wave interactions. *J. Fluid Mech.* **14** (4), 577–584.

BONTOZOGLOU, V. & HANRATTY, T. J. 1990 Capillary gravity Kelvin–Helmholtz waves close to resonance. *J. Fluid Mech.* **217**, 71–91.

CAMPBELL, B. K. 2009 Nonlinear effects on interfacial wave growth into slug flow. Master's thesis, Massachusetts Institute of Technology.

DOMMERMUTH, D. G. & YUE, D. K. P. 1987 A high-order spectral method for the study of nonlinear gravity-waves. *J. Fluid Mech.* **184**, 267–288.

DRAZIN, P. G. 1970 Kelvin–Helmholtz instability of finite amplitude. *J. Fluid Mech.* **42**, 321–335.

FAN, Z., LUSSEYRAN, F. & HANRATTY, T. J. 1993 Initiation of slugs in horizontal gas–liquid flows. *AIChE J.* **39** (11), 1741–1753.

FUNADA, T. & JOSEPH, D. D. 2001 Viscous potential flow analysis of Kelvin–Helmholtz instability in a channel. *J. Fluid Mech.* **445**, 263–283.

GASTER, M. 1962 A note on the relation between temporally-increasing and spatially-increasing disturbances in hydrodynamic stability. *J. Fluid Mech.* **14** (2), 222–224.

JANSSEN, P. 1986 The period-doubling of gravity capillary waves. *J. Fluid Mech.* **172**, 531–545.

JANSSEN, P. 1987 The initial evolution of gravity capillary waves. *J. Fluid Mech.* **184**, 581–597.

JURMAN, L. A., DEUTSCH, S. E. & MCCREADY, M. J. 1992 Interfacial mode interactions in horizontal gas–liquid flows. *J. Fluid Mech.* **238**, 187–219.

LIN, P. Y. & HANRATTY, T. J. 1986 Prediction of the initiation of slugs with linear-stability theory. *Intl J. Multiphase Flow* **12** (1), 79–98.

LOESCH, A. Z. 1974 Resonant interactions between unstable and neutral baroclinic waves. 1. *J. Atmos. Sci.* **31** (5), 1177–1201.

LONGUET-HIGGINS, M. S. 1962 Resonant interactions between two trains of gravity waves. *J. Fluid Mech.* **12**, 321–332.

LONGUET-HIGGINS, M. S. & COKELET, E. E. 1976 The deformation of steep surface waves on water. I. A numerical method of computation. *Proc. R. Soc. Lond.* A. **350**, 1–26.

MANSBRIDGE, J. V. & SMITH, R. K. 1983 On resonant interactions between unstable and neutral baroclinic waves. *J. Atmos. Sci.* **40** (2), 378–395.

MASLOWE, S. A. & KELLY, R. E. 1970 Finite-amplitude oscillations in a Kelvin–Helmholtz flow. *Intl J. Non-Linear Mech.* **5**, 427–435.

MATA, C., PEREYRA, E., TRALLERO, J. L & JOSEPH, DD 2002 Stability of stratified gas–liquid flows. *Intl J. Multiphase Flow* **28** (8), 1249–1268.

MCGOLDRICK, L. F. 1965 Resonant interactions among capillary-gravity waves. *J. Fluid Mech.* **21**, 305–331.

NAYFEH, A. H. & SARIC, W. S. 1972 Nonlinear waves in a Kelvin–Helmholtz flow. *J. Fluid Mech.* **55** (SEP26), 311–327.

PEDLOSKY, J. 1975 Amplitude of baroclinic wave triads and mesoscale motion in ocean. *J. Phys. Oceanogr.* **5** (4), 608–614.

PHILLIPS, O. M. 1960 On the dynamics of unsteady gravity waves of finite amplitude. 1. The elementary interactions. *J. Fluid Mech.* **9** (2), 193–217.

ROMANOVA, N. N. & ANNENKOV, S. Y. 2005 Three-wave resonant interactions in unstable media. *J. Fluid Mech.* **539**, 57–91.

TAITEL, Y. & DUKLER, A. E. 1976 Model for predicting flow regime transitions in horizontal and near horizontal gas–liquid flow. *AIChE J.* **22** (1), 47–55.

UJANG, P. M. 2003 Studies of slug initiation and development in two-phase gas–liquid pipeline flow. PhD thesis, University of London.

UJANG, P. M., LAWRENCE, C. J., HALE, C. P. & HEWITT, G. F. 2006 Slug initiation and evolution in two-phase horizontal flow. *Intl J. Multiphase Flow* **32** (5), 527–552.